Check for updates

ChemistrySelect

Research Article
doi.org/10.1002/slct.202302448

Chemistry Europe
European Chemical Societies Publishing

www.chemistryselect.org

# 3-Amino-thiophene-2-carbohydrazide Derivatives as Anti Colon Cancer Agents: Synthesis, Characterization, In-Silico and In-Vitro Biological Activity Studies

Halil Şenol*[a] and Furkan Çakır[b]

In this study, starting from 3-amino-thiophene-2-carboxylic acid methyl ester, eighteen new arylidenehydrazide derivatives (**4**–**21**) were synthesized. To determine cytotoxic activity of target compounds they were tested against human colon cancer and human umbilical vein endothelial cell lines. To determine prospective inhibition mechanism, binding affinity and complex stability molecular docking and molecular dynamics studies were carried out on transforming growth factor beta-2 (TGFβ2) and vascular endothelial growth factor receptor 2 (VEGFR2) proteins. According to the biological activity studies compounds *(E)*-2,4-dichloro-N-(2-(2-(4-fluorobenzylidene)hydrazine-1-carbonyl)thiophen-3-yl)benzamide (**11**) was found as the highest selective and active compound. Anti-cancer activity results compared to reference drugs doxorubicin and gefitinib. Most active compound was found as 7-fold and 4-fold more selective than doxorubicin and gefitinib, respectively. The detailed *in vitro* and *in silico* biological activity studies revealed that related compound demonstrated strong and selective anti-colon cancer effect and also it has promising inhibitory effects on TGFβ2 and VEGFR2. As a result, this compound is a promising candidate for further exploration and development in the field of colon cancer treatment.

## Introduction

Cancer is a disease in which cell growth and proliferation accelerate uncontrollably due to mutations and metastasize to other tissues besides the tissue in which it is located. Although treatment methods have improved, when the causes of death are taken into account, it is one of the leading causes, especially before the age of 70.[1] Considering that these rates are increasing every year, the number of people directly and indirectly affected by cancer increases, and as a result, it causes negativities in living standards and serious reductions in survival time. It was reported that almost 20 million people worldwide were affected by various types of cancer and about 10 million people died due to cancer. Among cancer types, colon cancer has a rate of 6% and rectum cancer has a rate of 3.8%.[2] TGF-β (Transforming Growth Factor Beta) regulates cell growth, differentiation, and apoptosis. This factor has been observed to be impaired in many types of cancer, especially colorectal cancer, and it is thought to play a role in cancer formation. Overexpression of TGF-β2 has been associated with advanced cancer and has been shown to induce metastasis and worsen the prognosis in colon cancer patients. In addition, TGF-β2 induces angiogenesis in cancer tissue, increasing the oxygen and nutrient delivery to the tumor tissue, leading to tumor growth and acceleration of metastasis. So, TGF-β2 has a crucial importance in colorectal cancer due to its many other cancer-supporting roles.[3,4]

In the past decade, molecular docking and molecular dynamics studies have significantly influenced drug discovery. Molecular docking is a computational technique used to predict the interaction between the targeted ligand and the protein. Molecular dynamics studies, as the continuation of molecular docking studies, is the *in-silico* method used to determine the stability of the ligand-receptor complex. In addition, drug ADME properties and drug-likeness can be investigated by *in-silico* methods to determine druggability. Molecular modeling methods provide a foresight of the biological activities of new agents, and they are undoubtedly advantageous in identifying potential drug molecules among these agents.[5]

Thiophene is a five-membered sulfur bearing heterocyclic aromatic compound. Some known drug contains thiophene ring (Figure 1). Tinoridine is an anti-inflammatory drug with having thiophene ring. OSI-930, whose clinical researches are continuing as anti-cancer agents.[6,7] Lomibuvir is a 3-amino-

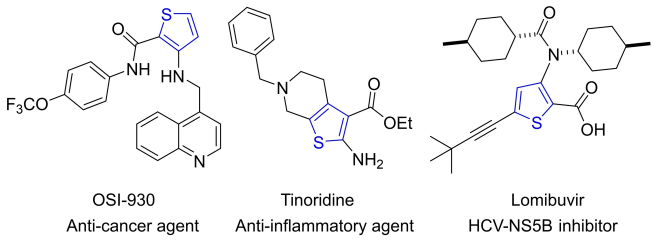


**Figure 1.** Some known drugs having thiophene ring.

[a] *Dr. H. Şenol*
*Department of Pharmaceutical Chemistry*
*Bezmialem Vakif University, Faculty of Pharmacy*
*34093, Fatih, Istanbul, Türkiye*
*E-mail: hsenol@bezmialem.edu.tr*

[b] *F. Çakır*
*Bezmialem Vakif University, Faculty of Pharmacy*
*34093, Fatih, Istanbul, Türkiye*

*Supporting information for this article is available on the WWW under https://doi.org/10.1002/slct.202302448*



© 2023 Wiley-VCH GmbH

Research Article
doi.org/10.1002/slct.202302448
Chemistry Europe
European Chemical Societies Publishing

thiophene-2-carboxylic acid derivative having HCV-NS5B inhibitory activity.[8]

Arylidenehydrazide derivatives have various biological activity such as anti-cancer,[9,10] anti-bacterial,[11] anti-inflammatory,[12] anti-fungal,[13] analgesic,[14] anti-convulsant,[14] anti-malarial[15] and anti-tubercular.[16]

The aim of this study is the discovery of new selective and potential anti-cancer agents. For this purpose, starting from 3-amino-thiophene-2-carboxylic acid methyl ester, eighteen new arylidenehydrazide derivatives (**4**–**21**) were synthesized and investigated their cytotoxic effects against HCT116 and HUVEC cell lines. Furthermore, molecular docking and molecular dynamics studies were carried out to determine ligand-protein interactions and the stability of the ligand-protein complexes. All the synthesized compounds were purified by chromatographic methods and/or crystallization. Then the structures of all the synthesized compounds were very well characterized by spectroscopic analysis.

## Results and Discussion

### Synthesis of Target Compounds

The synthetic route of the target compounds was described in Scheme 1. Initially, compound **1** was converted to corresponding amide (**2**) using 2,4-dichloro benzoyl chloride in the presence of $NaHCO_3$ in DCM.[17] The ester group of compound **2** was converted to related hydrazide (**3**) using hydrazine hydrate and a catalytic amount of PTSA in ethanol at high temperature.[9] Finally, hydrazide compound (**3**) was reacted with eighteen different aromatic aldehydes, separately, in the presence of a catalytic amount of HOAc in ethanol at high temperature. So, all the target compounds were synthesized (**4**–**21**).

In our preliminary molecular docking studies, we noticed interesting observations and interactions regarding the 2,4-dichlorophenyl ring as an amide structure and the fluorinated phenyl ring as an arylidenehydrazide moiety. Therefore 2,4-dichlorobenzoyl chloride and especially halogenated aldehydes were selected to synthesize of target compounds. Interestingly, 2,4-dichlorobenzoyl moiety exhibited two halogen bond interactions in addition to other polar interactions with the amino acid residues. All the synthesized compounds were purified by chromatographic or/and crystallization methods and their

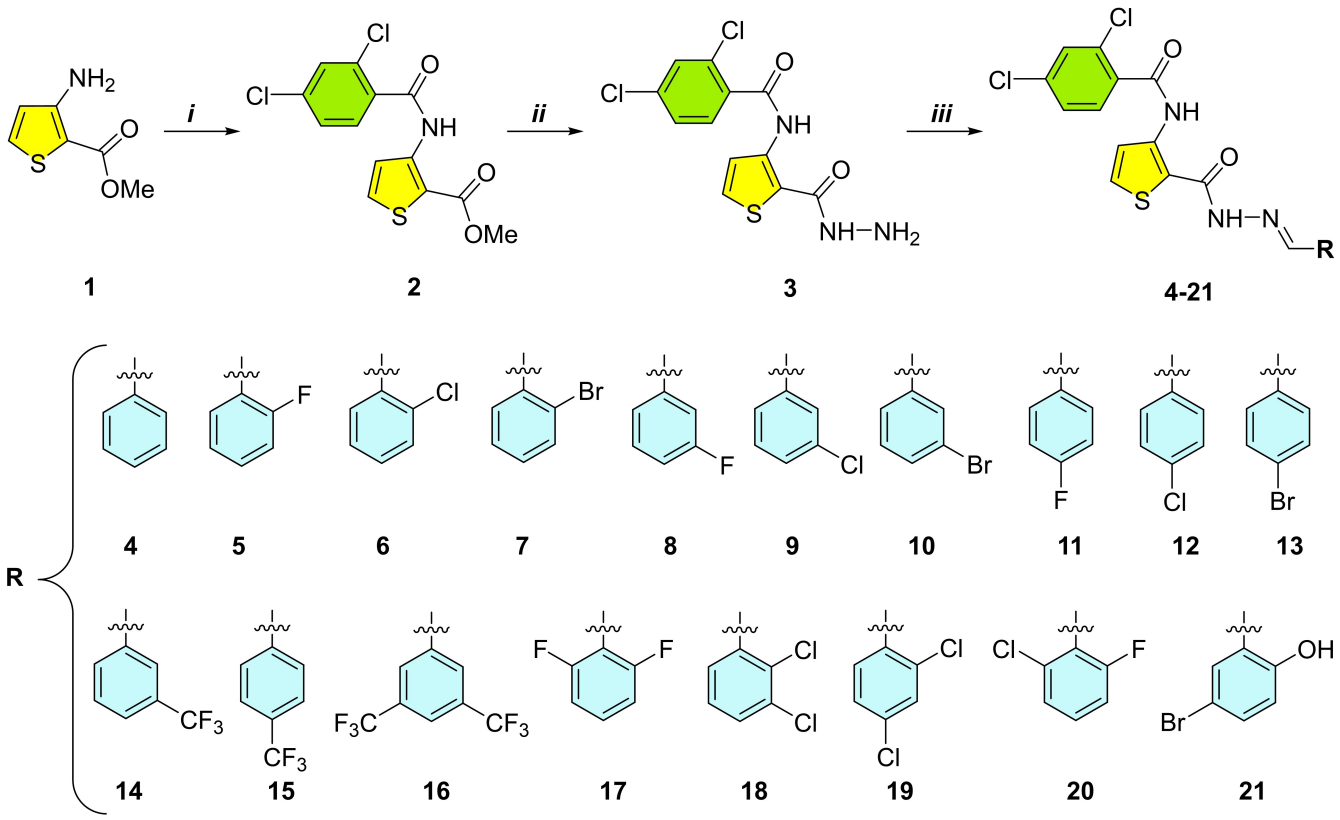


***Reagents and Conditions: i)*** 2,4-dichlorobenoyl chloride, $NaHCO_3$, DCM, rt, overnight;

***ii)*** $NH_2NH_2.H_2O$, EtOH, PTSA, reflux, overnight; ***iii)*** Corresponding aldehyde, EtOH, HOAc, reflux, 1h.

**Scheme 1.** Synthesis of target compounds.


© 2023 Wiley-VCH GmbH

23656549, 2023, 39, Downloaded from https://chemistry-europe.onlinelibrary.wiley.com/doi/10.1002/slct.202302448 by Bezm-I Alem Vakif University, Wiley Online Library on [01/11/2023]. See the Terms and Conditions (https://onlinelibrary.wiley.com/terms-and-conditions) on Wiley Online Library for rules of use; OA articles are governed by the applicable Creative Commons License

Research Article
doi.org/10.1002/slct.202302448
Chemistry Europe
European Chemical Societies Publishing

structures were very well characterized by NMR, FT-IR, and ESI-HRMS analysis.

### Structure Characterization

In the $^{1}$H NMR spectrum of compound **2**, the NH proton resonated at 10.68 ppm as singlet. The signals of ester and amide carbonyls of compound **2** were detected at 164.63, 162.94 ppm, respectively, in $^{13}$C APT NMR spectrum with the help of and HMBC analysis. The ester methoxy resonated at 3.80 and 52.10 ppm in $^{1}$H NMR and $^{13}$C APT NMR spectra, respectively. After the conversion of the ester group to hydrazide, the methoxy signal lost from both $^{1}$H NMR and $^{13}$C APT NMR spectra. Furthermore, the hydrazide carbonyl resonated at 163.5 ppm in $^{13}$C APT NMR spectrum and the CONH proton of hydrazide resonated at 9.09 ppm in $^{1}$H NMR spectrum. Finally, the amide hydrogen of compound **3** resonated at 12.58 ppm.

In the $^{1}$H NMR spectra of all arylidenehydrazide compounds the imine proton was observed around 8.1–8.6 ppm as a broadened singlet, and in the $^{13}$C APT NMR spectra the imine carbon resonated around 143–144 ppm.[10,18,19] In the fluorinated derivatives **(5, 8, 11, 14–17, 20)** fluorine atom split the signals of adjacent carbon to n+1 (n=number of fluorine) signals in the $^{13}$C APT NMR spectra (Figures 2 and 3). The effect of a fluorine atom extends to the adjacent carbons up to a distance of four bonds.[20] The detailed $^{13}$C APT NMR spectrum and peak splitting caused by the fluorine of compound **5** was given in Figure 2.

While compounds **14–16** have $CF_3$ groups, other fluorinated derivatives have one or two F atoms on aromatic ring. The carbon which is attached to F in compound **5** resonated at 161.33 ppm as doublet *(162.33, 160.33)* with 250.5 Hz coupling constant (Figure S18). The imine carbon of compound **5** was split by fluorine, at three bonds distance, as doublet in the $^{13}$C APT NMR spectrum. Interestingly, in compound **17**, although the 2,6-difluorophenyl ring has free rotation, fluorine-attached carbons resonated at 160.64 (d, $J$=255.2 Hz, *161.67, 159.65*), and 160.60 (d, $J$=255.2 Hz, *161.63, 159.60*) ppm which is a slight difference (Figure S82).

In compound **8** (3-fluorophenyl derivative), while the carbons at the ortho positions of fluorine resonated at 117.41 (d, $J$=21.4 Hz, *117.49, 117.32*) and 113.87 (d, $J$=22.8 Hz, *113.96, 113.78*) ppm, the carbons at the meta positions resonated at 131.50 (d, $J$=8.1 Hz, *131.53, 131.47*) and 136.85 (ipso, d, $J$=7.6 Hz, *136.88, 136.82*) ppm in the $^{13}$C APT NMR spectrum (Figure S33). In the $CF_3$ substituted derivatives **(14–16)**, the

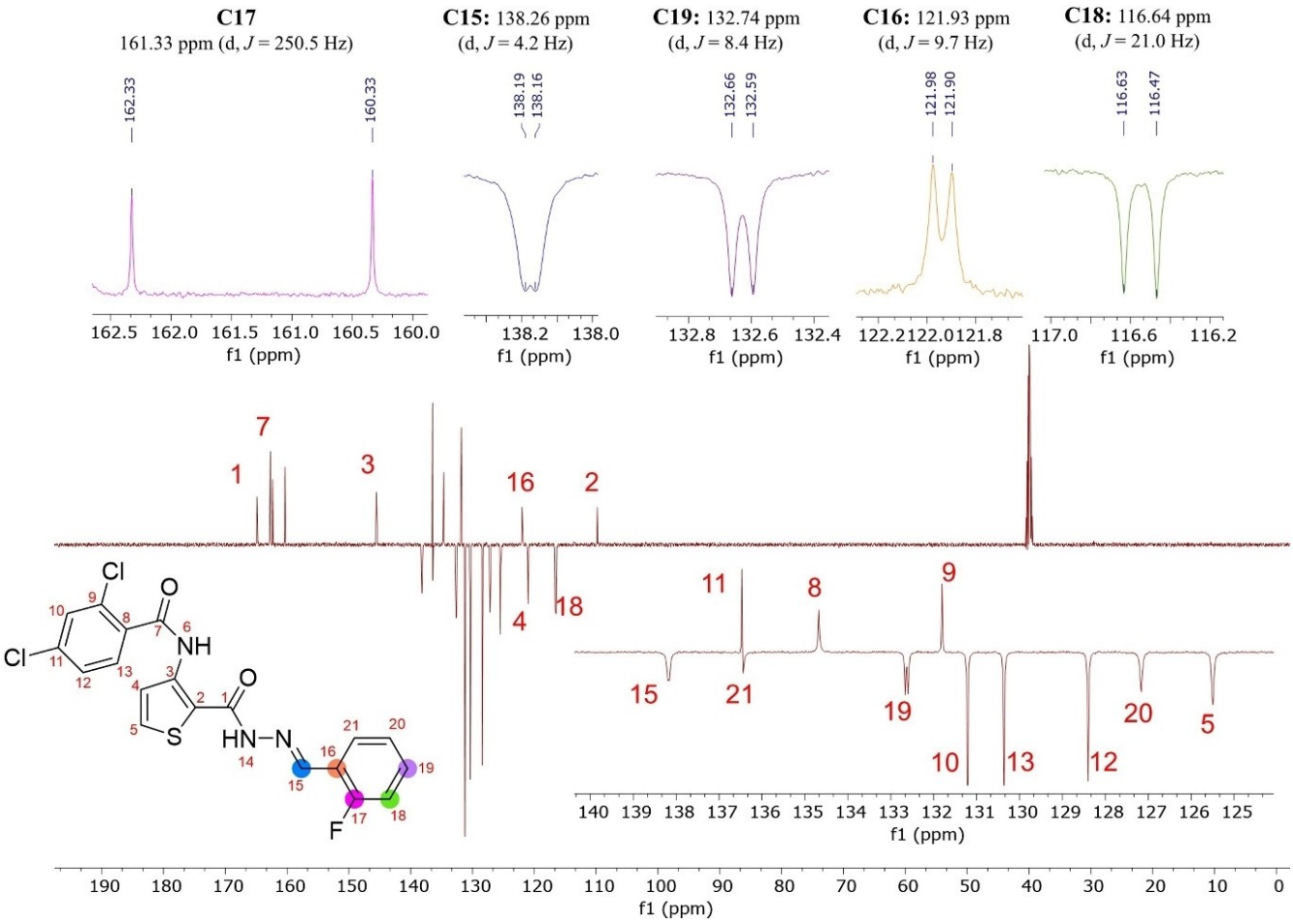


**Figure 2.** The detailed $^{13}$C APT NMR spectrum and peak splitting's caused by the fluorine in compound **5**.


© 2023 Wiley-VCH GmbH

23656549, 2023, 39, Downloaded from https://chemistry-europe.onlinelibrary.wiley.com/doi/10.1002/slct.202302448 by Bezm-I Alem Vakif University, Wiley Online Library on [01/11/2023]. See the Terms and Conditions (https://onlinelibrary.wiley.com/terms-and-conditions) on Wiley Online Library for rules of use; OA articles are governed by the applicable Creative Commons License

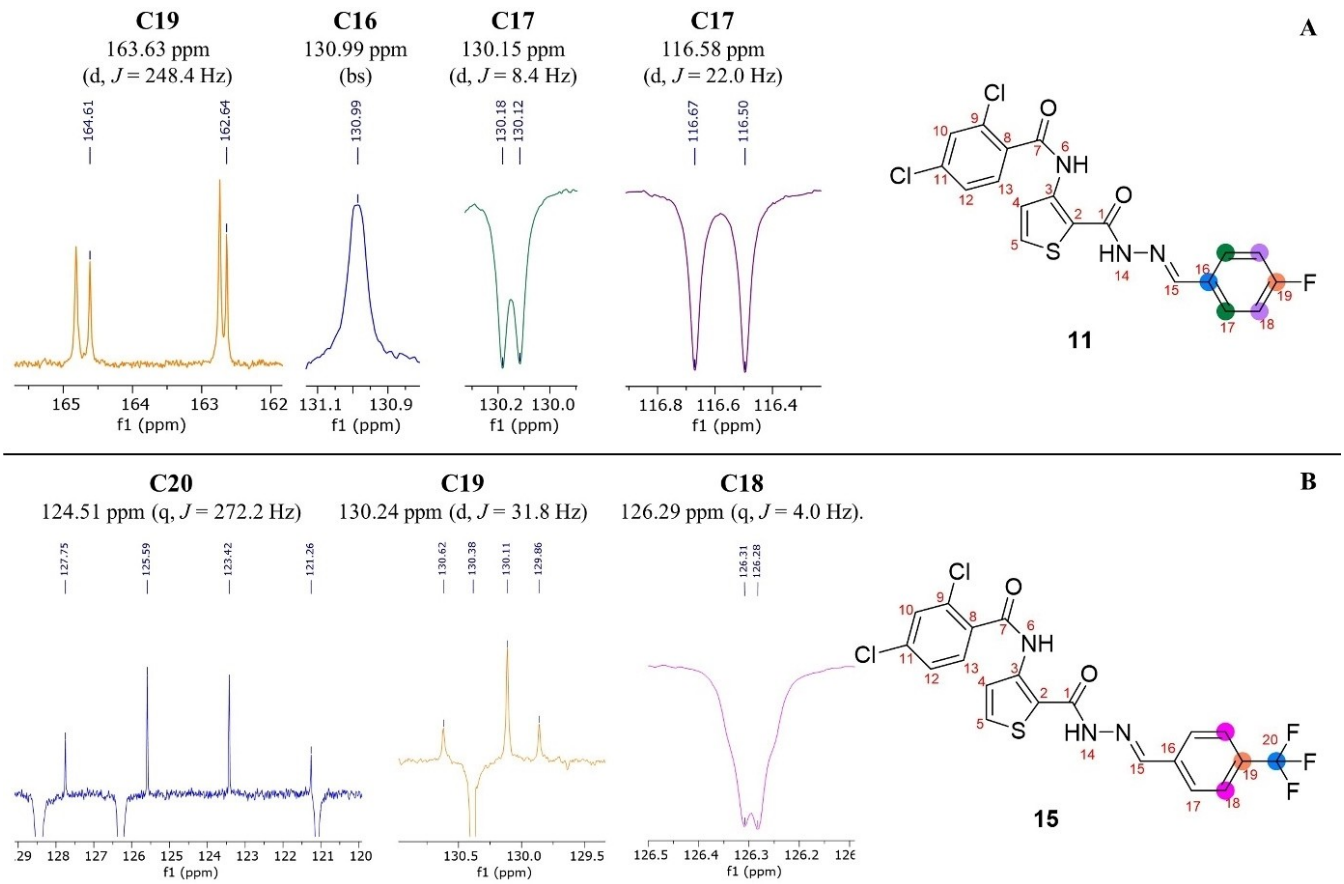


**Figure 3.** The $^{13}$C APT NMR spectra peak splitting's with coupling constants caused by the fluorine in compounds **11** (A) and **15** (B).

carbon of $CF_3$ resonated around 125 ppm as quartet with a 272 Hz coupling constant in the $^{13}$C APT NMR spectra (Figure 3B). $^{19}$F NMR analysis was also carried out for the characterization of fluorinated compounds. While the $CF_3$ groups of compounds **14**–**16** resonated as singlets at −61 ppm in the $^{19}$F NMR (Figures S66, S72, and S78), the signals of fluorine's attached to aromatic ring resonated at different ppm's from −108 to −120 ppm.

As seen in ESI-HRMS spectra the exact monoisotopic masses (m/z) of all the synthesized compounds were found maximum in ±0.4% precision. While in brominated derivatives, the monoisotopic masses were found using $^{81}$Br in HRMS spectra, in some of the chlorinated derivatives $^{37}$Cl was used.

### In vitro Cytotoxicity Studies

To determine cytotoxic activity and selectivity, all the synthesized target compounds **(4–21)** were tested against human colon cancer cell (HCT116) and human umbilical vein endothelial cell (HUVEC) lines and results were given in Table 1.

Doxorubicin and gefitinib were used as reference anticancer drugs to compare new compounds. When evaluated the cytotoxic effects of target compounds against HCT116 cell lines, the most effective compounds were found as **11** (5.28 μM), **17** (8.97 μM), **5** (11.47 μM), and **15** (12.29 μM). In addition, the cytotoxic effects of the most active compounds against HUVEC cell line were found as 171.60 μM for compound **11**, 118.90 μM for compound **17**, 114.60 μM for compound **15**, and 85.44 μM for compound **5**. The selectivities of the most active compounds were calculated from the equation of Selectivity Index (SI) = $IC_{50}$Huvec/$IC_{50}$HCT116.

According to the *in vitro* cytotoxicity result the most selective compounds were found as **11** (SI: 32.4), **17** (SI: 13.3), **15** (SI: 9.3) and **5** (SI: 7.72). On the other hand, the cytotoxic effects of doxorubicin (Dox.) and gefitinib (Gef.) against HCT116 cells were found as 1.97 and 13.48 μM, respectively. The similar results were obtained by other studies.[21,22] Doxorubicin was found to be more active than all the synthesized compounds, but its cytotoxic effects against HUVEC cells were higher than all the other compounds. So, selectivity of doxorubicin (SI: 4.60) is lower than the most active new compounds. The selectivity of gefitinib was found as 7.60. Compound **11** was found as 7-fold and 4-fold more selective than doxorubicin and gefitinib, respectively. Additionally, while compounds **17** and **15** were found as 3-fold and 2-fold more selective than doxorubicin, respectively, compound **17** is 1.7-fold more selective than gefitinib. On the other hand, while compounds **8, 14, 16, 20** and **21** showed moderate cytotoxicity and selectivity against


© 2023 Wiley-VCH GmbH

23656549, 2023, 39, Downloaded from https://chemistry-europe.onlinelibrary.wiley.com/doi/10.1002/slct.202302448 by Bezm-I Alem Vakif University, Wiley Online Library on [01/11/2023]. See the Terms and Conditions (https://onlinelibrary.wiley.com/terms-and-conditions) on Wiley Online Library for rules of use; OA articles are governed by the applicable Creative Commons License

**Table 1.** The cytotoxic effects and selectivity indexes of target compounds.

| | HCT116 | | HUVEC | | Selectivity Index |
|---|---|---|---|---|---|
| Cpd. | $IC_{50}$ [μM] | $r^2$ | $IC_{50}$ [μM] | $r^2$ | HUVEC/HCT116 |
| **4** | 53.79 ± 0.88 | 0.9264 | 45.76 ± 1.54 | 0.9440 | 0.85 |
| **5** | 11.47 ± 0.28 | 0.9718 | 85.44 ± 2.03 | 0.9590 | 7.72 |
| **6** | 58.95 ± 0.97 | 0.9459 | 52.19 ± 1.63 | 0.9492 | 0.89 |
| **7** | 41.09 ± 0.72 | 0.9315 | 71.82 ± 1.76 | 0.9563 | 1.73 |
| **8** | 18.56 ± 1.98 | 0.7606 | 97.03 ± 2.18 | 0.9451 | 5.38 |
| **9** | 76.54 ± 2.14 | 0.9502 | 75.48 ± 1.89 | 0.9833 | 0.98 |
| **10** | 142.80 ± 4.14 | 0.9811 | 57.43 ± 2.63 | 0.9478 | 0.40 |
| **11** | 5.28 ± 0.38 | 0.9860 | 171.60 ± 3.96 | 0.9155 | 32.38 |
| **12** | 52.21 ± 1.08 | 0.9680 | 61.71 ± 1.25 | 0.9605 | 1.17 |
| **13** | 102.80 ± 2.54 | 0.9235 | 75.75 ± 1.92 | 0.9781 | 0.73 |
| **14** | 16.80 ± 1.05 | 0.8481 | 108.01 ± 2.31 | 0.9899 | 6.42 |
| **15** | 12.29 ± 0.28 | 0.9285 | 114.60 ± 3.35 | 0.9757 | 9.26 |
| **16** | 19.5 ± 0.74 | 0.9366 | 68.90 ± 1.83 | 0.9581 | 5.60 |
| **17** | 8.97 ± 0.63 | 0.9702 | 118.90 ± 2.28 | 0.9774 | 13.25 |
| **18** | 38.66 ± 1.98 | 0.9668 | 57.13 ± 2.64 | 0.9320 | 1.51 |
| **19** | 33.40 ± 1.81 | 0.9794 | 63.23 ± 1.75 | 0.9275 | 1.91 |
| **20** | 28.45 ± 1.48 | 0.9785 | 111.30 ± 2.30 | 0.9894 | 3.96 |
| **21** | 14.84 ± 1.20 | 0.9261 | 80.41 ± 1.99 | 0.9451 | 5.71 |
| Gef. | 13.48 ± 0.80 | 0.9415 | 102.50 ± 3.25 | 0.9510 | 7.60 |
| Dox. | 1.97 ± 0.11 | 0.9335 | 9.06 ± 0.11 | 0.9765 | 4.60 |

HCT116 and HUVEC cell lines, the rest of the compounds did not show reasonable activity and selectivity.

The results emphasize the potential advantages of the newly synthesized compounds as anti-cancer agents. The new compounds demonstrated higher cytotoxicity against HCT116 cancer cells compared to the reference drugs doxorubicin and gefitinib, indicating their potential to effectively target and eliminate cancer cells. The compounds exhibited a remarkable selectivity for cancer cells over normal cells (HUVEC). This suggests that they might have a reduced impact on healthy cells, minimizing potential side effects. The calculated SI values highlight the compounds' specificity for cancer cells. Particularly, compound **11** displayed an exceptionally high SI, indicating its strong potential as a selective anti-cancer agent. Compound **11** was notably more selective than both doxorubicin and gefitinib. Similarly, compounds **17** and **15** exhibited higher selectivity than doxorubicin and gefitinib.

In summary, the newly synthesized compounds, especially compounds **11**, **15**, and **17**, showed promising anti-cancer activity with significantly improved selectivity compared to traditional reference drugs. These findings suggest that these compounds have the potential to be developed into effective and targeted anti-cancer treatments.

## Molecular Docking Studies

To evaluate the prospective inhibition mechanism of synthesized compounds, molecular docking studies were carried out against two different receptor proteins that are related to cancer cell growth. The selected proteins are TGF-β2 and VEGFR2. The X-ray crystallographic structure of the proteins which are 5QIN for TGFβ2 and 4ASE for VEGFR2 were provided by Protein Data Bank. The compounds **(5, 11, 15**, and **17)** that are more active than both reference drugs as *in vitro* were selected and they were docked related proteins separately and binding scores were determined between ligands and proteins. In addition, MM-GBSA ΔG binding free energies of ligand-protein complexes were calculated. The molecular docking scores and MM-GBSA ΔG binding free energies of the chosen compounds against related proteins were given in Table 2.

**Table 2.** Molecular docking scores and MM-GBSA ΔG binding free energies of *in vitro* most active compounds (kcal/mol).

| | TGFβ2 (PDB ID: 5QIN) | | VEGFR2 (PDB ID: 4ASE) | |
|---|---|---|---|---|
| Copd. | Docking Scores | MM-GBSA ΔG Bind | Docking Scores | MM-GBSA ΔG Bind |
| **5** | −9.023 | −62.67 | −9.340 | −50.72 |
| **11** | −11.310 | −60.06 | −9.555 | −55.79 |
| **15** | −10.132 | −54.73 | −9.733 | −60.61 |
| **17** | −11.604 | −58.32 | −9.366 | −50.58 |


© 2023 Wiley-VCH GmbH

23656549, 2023, 39, Downloaded from https://chemistry-europe.onlinelibrary.wiley.com/doi/10.1002/slct.202302448 by Bezm-I Alem Vakif University, Wiley Online Library on [01/11/2023]. See the Terms and Conditions (https://onlinelibrary.wiley.com/terms-and-conditions) on Wiley Online Library for rules of use; OA articles are governed by the applicable Creative Commons License

Research Article
doi.org/10.1002/slct.202302448
Chemistry Europe
European Chemical Societies Publishing

According to the molecular docking studies, compounds **11** and **17** were found as the best inhibitors of TGFβ2 with docking scores of −11.310 and −11.604 kcal/mol, respectively. On the other hand, compound **15** was found as the best inhibitor for the VEGFR2 with a −9.733 kcal/mol docking score, while compound **11**, which of the best inhibitors of TGFβ2, demonstrated similar inhibition against VEGFR2 (−9.555 kcal/mol). Compound **11** was found to be the second-best inhibitor of both target proteins.

The MM-GBSA ΔG binding free energy results showed that compounds **11** and **17** have −60.06 and −58.32 kcal/mol binding affinity against TGFβ2, respectively. On the other hand, for the VEGFR2 the MM-GBSA ΔG binding free energies of compounds **11** and **15** were found as −55.79 and −60.61 kcal/mol, respectively (Table 2). MM-GBSA ΔG binding free energy is important for molecular docking studies. It provides a prediction of the binding affinity of ligand-protein complexes. Additionally, it helps in the selection of leading compounds by evaluating the effect of structural modifications on binding affinity.[23]

The molecular docking 2D interactions between TGFβ2 (5QIN) and compounds **11** and **17** were given in Figure 4 and also 3D interactions between TGFβ2 and compounds **11** and **17** were given in Figure 5. Considering the complexes between TGFβ2 and compounds **11** and **17**, the hydrogen bond between the Asn-332 and the carbonyl oxygen of the amide group formed as well as halogen bond interactions between the Asp-397 and the chloride in the para position of the amide functional group. Interestingly, compound **17** exhibits two more halogen bond interactions with Asn-332 and Lys-252 (Figure 4).

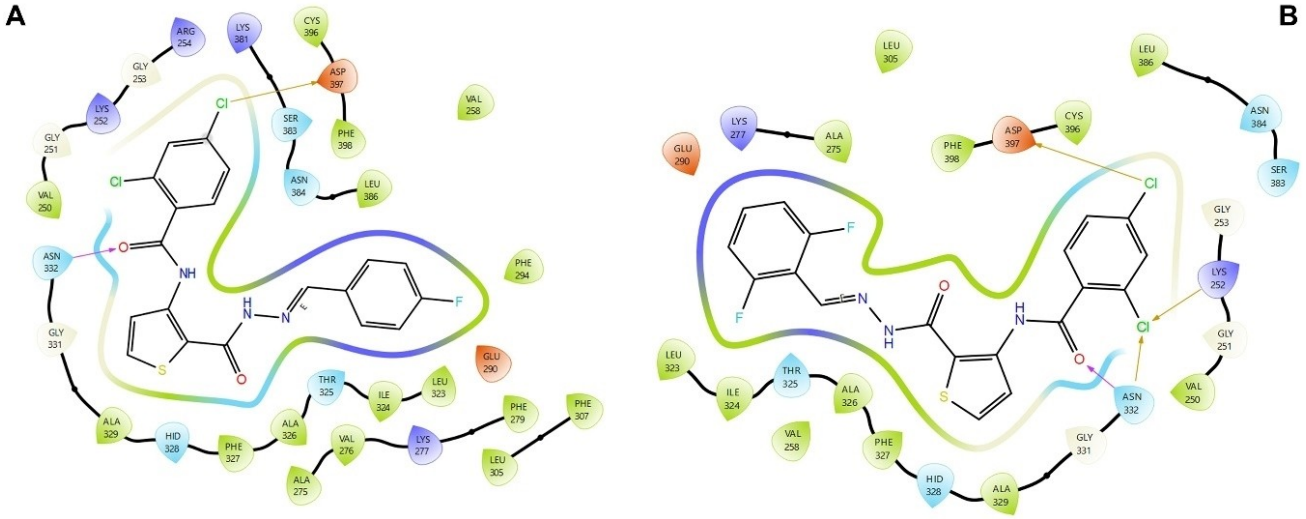


**Figure 4.** Molecular docking 2D ligand-protein interactions between active site of TGFβ2 and compounds **11** (A) and **17** (B).

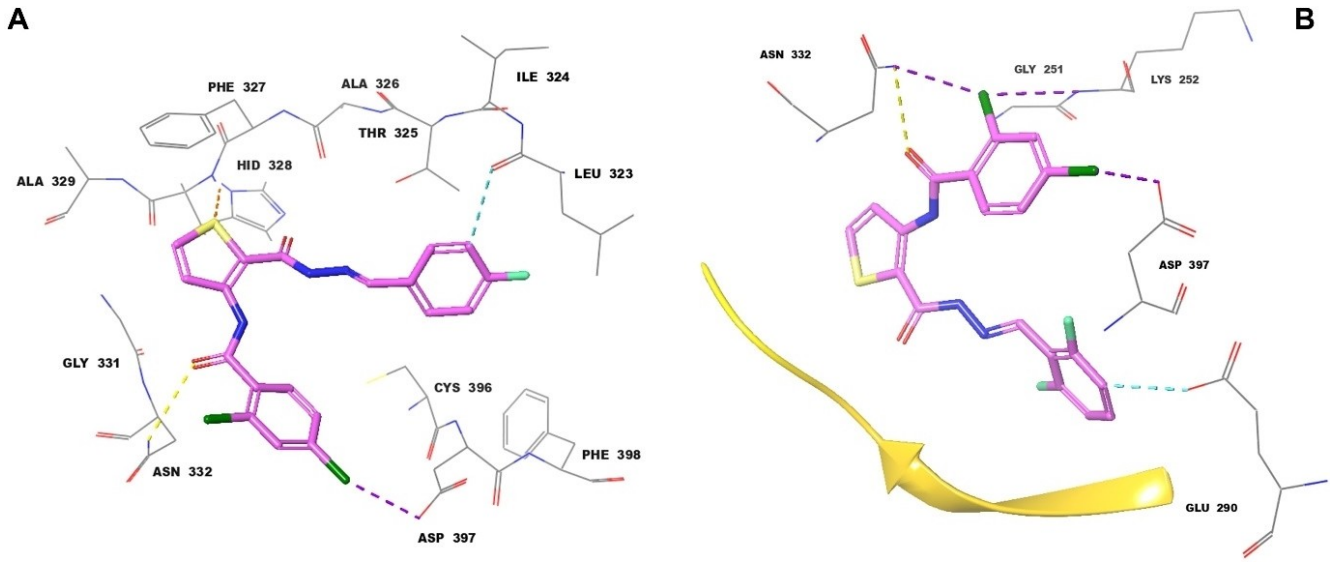


**Figure 5.** Molecular docking 3D ligand-protein interactions between active site of TGFβ2 and compounds **11** (A) and **17** (B).


© 2023 Wiley-VCH GmbH

23656549, 2023, 39, Downloaded from https://chemistry-europe.onlinelibrary.wiley.com/doi/10.1002/slct.202302448 by Bezm-I Alem Vakif University, Wiley Online Library on [01/11/2023]. See the Terms and Conditions (https://onlinelibrary.wiley.com/terms-and-conditions) on Wiley Online Library for rules of use; OA articles are governed by the applicable Creative Commons License

On the other hand, while an aromatic hydrogen bond interaction formed between the ortho position of the fluorine and the carbonyl oxygen of the Leu-323 between compound **11** and TGFβ2, the same interaction was observed between Glu-290 and the meta position of the hydrazone structure of compound **17**. In Figure 5, the yellow dashes represent hydrogen bond interactions, turquoise dashes represent aromatic hydrogen bond interactions, and the purple dashes represent halogen bond interactions. The distances between interacted ligand atoms and amino acid residues were measured and the bond strengths were discussed. In the **TGFβ2-11** and **TGFβ2-17** complexes, the lengths of the hydrogen bond between carbonyl oxygen and Asn-332 were measured as 3.06 Å and 3.11 Å, respectively.

The molecular docking 2D ligand-protein interactions between VEGFR2 (4ASE) and compounds **11** and **17** were given in Figure 6 and also 3D ligand-protein interactions were given in Figure 7.

As demonstrated in Figure 6A complex between VEGFR2 and compound **11** was conducted via hydrogen bond, halogen bond, and pi-cation interactions. As the main structure of the synthesized compounds thiophene ring showed pi-cation interaction with Lys-868. As a negatively charged amino acid Asp-1046 interacted with the nitrogen of the hydrazone structure and the oxygen of the hydrazide carbonyl via a hydrogen bond. In addition, the chlorine of the ortho position of amide carbonyl formed two different halogen bond interactions with Cys-919 and Glu-917. Same as with compound **11**, compound **15** interacted with Lys-868 and Asp-1046 with pi-cation and hydrogen bonds. But, when compared, even though the interaction formed with Asp-1046 is still a hydrogen bond, the interaction hosts a difference. While compound **11** (Figure 6A) formed the hydrogen bonds with its carbonyl

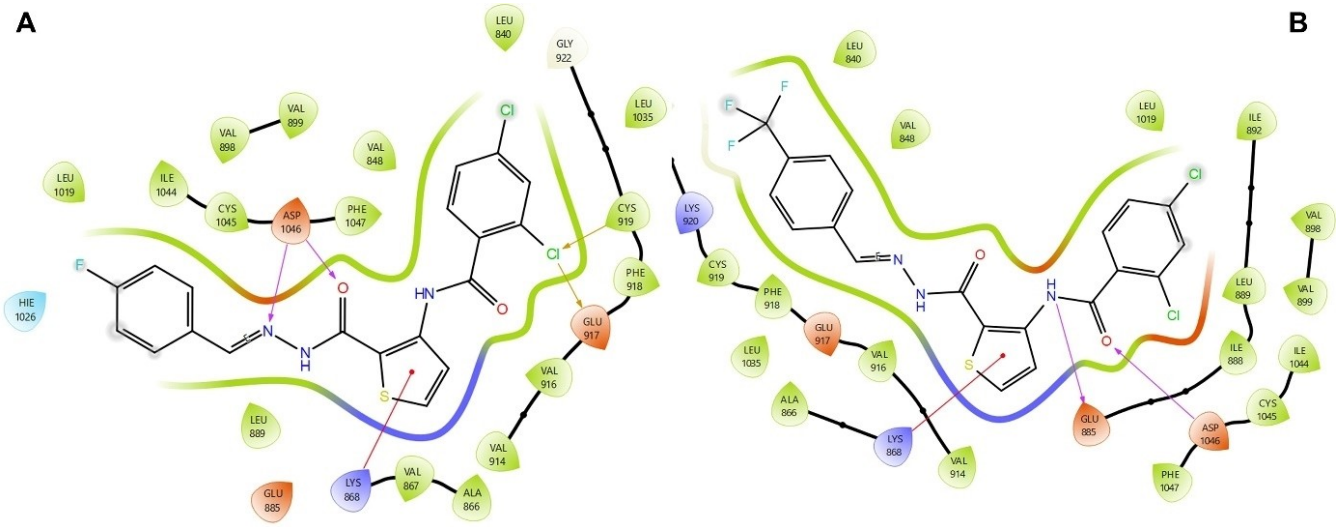


**Figure 6.** Molecular docking 2D ligand-protein interactions between active site of VEGFR2 and compounds **11** (A) and **15** (B).

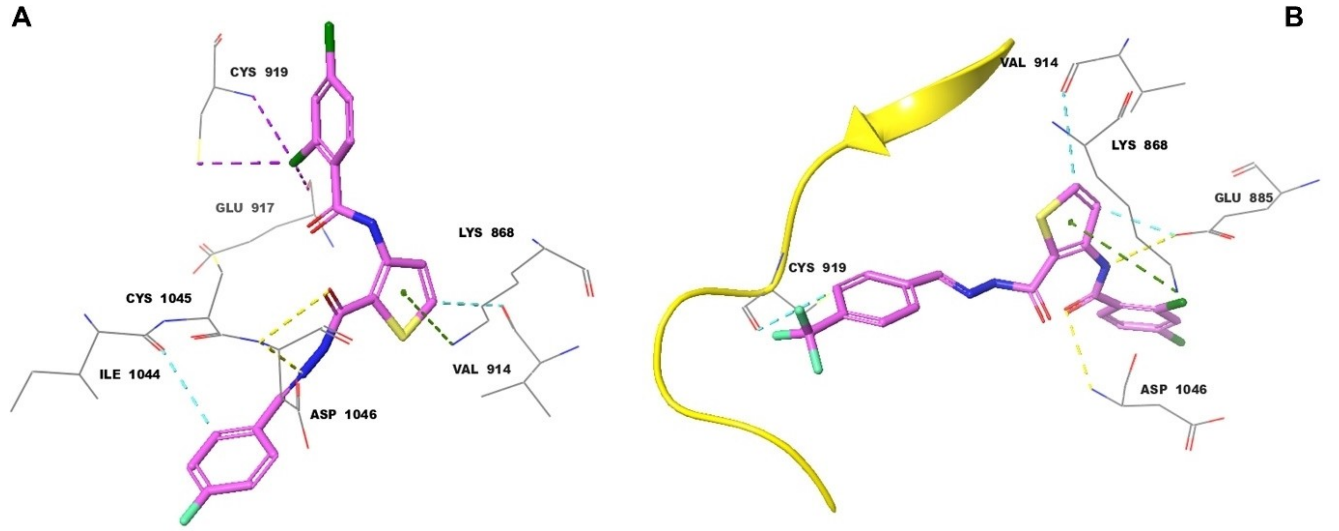


**Figure 7.** Molecular docking 3D ligand-protein interactions between active site of VEGFR2 and compounds **11** (A) and **15** (B).


© 2023 Wiley-VCH GmbH

23656549, 2023, 39, Downloaded from https://chemistry-europe.onlinelibrary.wiley.com/doi/10.1002/slct.202302448 by Bezm-I Alem Vakif University, Wiley Online Library on [01/11/2023]. See the Terms and Conditions (https://onlinelibrary.wiley.com/terms-and-conditions) on Wiley Online Library for rules of use; OA articles are governed by the applicable Creative Commons License

oxygen of hydrazide and the nitrogen of hydrazone structure, compound **15** interacted with its carbonyl oxygen of amide structure. Differently, another hydrogen bond formed between the amide nitrogen of compound **15** and Glu-885. In addition, pi-cation interaction was also seen between the thiophene ring and Lys-868 (Figure 6B).

As seen in 3D ligand protein interactions of VEGFR2 and compound **11** (Figure 7A), in addition to halogen bond (purple dashes), pi-cation (green dashes), and hydrogen bond (yellow dashes), aromatic hydrogen bonds were also seen. The halogen bonds were measured between 2.88–3.52 Å. The hydrogen bonds between Cys-1045 and hydrazone nitrogen and Cys-1045 and carbonyl oxygen were measured as 2.97 Å and 3.28 Å, respectively. Finally, the aromatic hydrogen bond between the thiophene ring and Val-914 was measured as 3.26 Å while the length of the aromatic bond interaction between the Cys-1045 and meta position of the fluorine is 3.52 Å. These results may be a representative of stable ligand-protein complex.

As seen in Figure 7B, hydrogen bonds (yellow dashes), aromatic hydrogen bonds (turquoise dashes), and pi-cation interactions were observed in 3D interactions between VEGFR2 and **15**. While the length of the aromatic hydrogen bond between the fourth position of the thiophene ring and Glu-885 is 2.96 Å, it was 3.50 Å between the fifth position of the thiophene ring and Val-914. Moreover, Cys-919 of the VEGFR2 protein interacted with the ortho position of trifluoromethyl of the compound **15** via an aromatic hydrogen bond with a length of 3.52 Å. Furthermore, lengths of hydrogen bond interactions were also measured. The oxygen of the amide carbonyl interacted with Asp-1046 with a 2.96 Å bond length, while the hydrogen bond interaction was measured as 3.03 Å between the nitrogen of amide structure and Glu-885.

## Molecular Dynamics Studies

To determine the stability of ligand-protein complexes molecular dynamics studies were carried out for **TGFβ2-11, TGFβ2-17, VEGFR2-11** and **VEGFR2-15** ligand protein complexes. In addition, the RMSD (root mean square deviation) values of ligand atoms and proteins were calculated. According to the RMSD values and key interactions obtained from MD simulations of ligand-protein complexes the most active complex were determined.

## MD Simulations on TGFβ2

The ligand-protein 2D key interactions with simulation times of **TGFβ2-11** and **TGFβ2-17** complexes were given in Figure 8.

As can be seen from Figure 8A, compound **11** formed direct hydrogen bond interactions with His-328 (87% of simulation time) and Asn-332 (89% of sim.). In addition, there are two different water-bridged hydrogen bond interactions between Val-250 and hydrazone (59% of sim.) and also between Val-250 and amide nitrogen (47% of sim.). Finally, the thiophene ring formed a weak pi-pi stacking interaction with Phe-327 (12% of sim.). The key interactions are hydrogen bonds and they were observed more than 85% of the simulation time. As seen in Figure 8B, compound **17** showed an intramolecular hydrogen bond between amide carbonyl and hydrazide N–H during 79% of the simulation time. Furthermore, amide N–H formed a hydrogen bond interaction with Val-250 (72% of sim.). In addition, there were four water-bridged hydrogen bond interactions with a different simulation time between Ala-326 (25% of sim.), His-328 (58% and 17% of sim.) and Thr-325 (13% of sim).

Figure 9 demonstrated that both complexes are very stable, but the **TGFβ2-17** complex is more stable than **TGFβ2-11** because the RMSD values of the ligand atoms and protein Cα atoms were calculated to average 1.2 Å and 2.4 Å, respectively. The RMSD value belonging to the ligand deviation from its reference conformation was found as 0.8 Å. If this value is lower than 2 Å, the docking validation is acceptable.

Ligand-protein interactions can be monitored throughout the simulation. These interactions can be categorized as hydro-

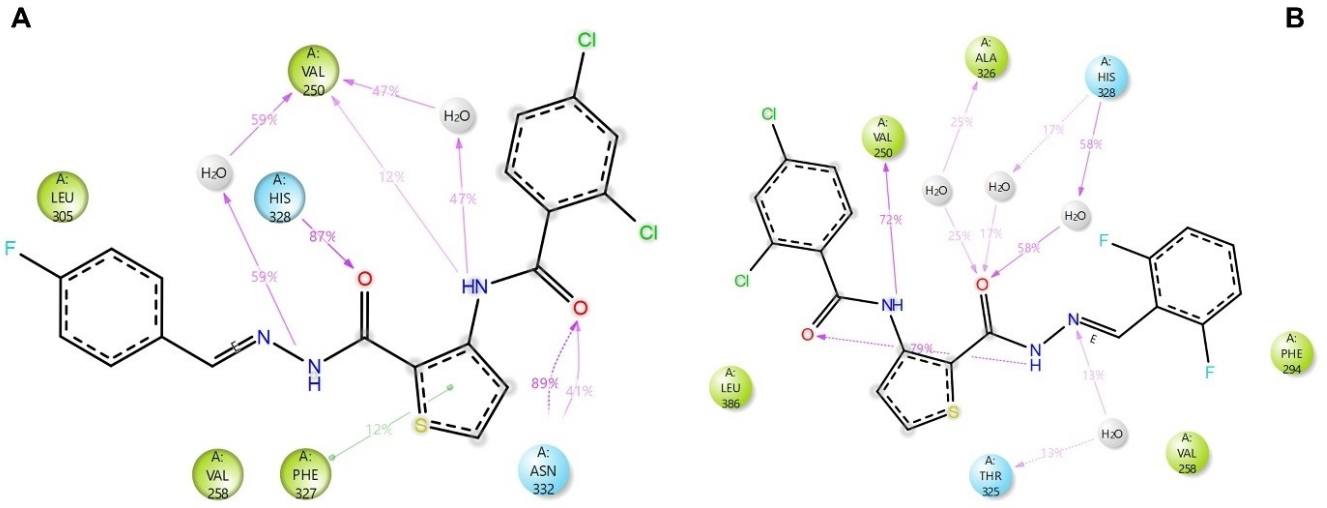


**Figure 8.** The MD ligand-protein 2D key interactions with % of simulation time of **TGFβ2-11** (A) and **TGFβ2-17** (B) complexes.


© 2023 Wiley-VCH GmbH

23656549, 2023, 39, Downloaded from https://chemistry-europe.onlinelibrary.wiley.com/doi/10.1002/slct.202302448 by Bezm-I Alem Vakif University, Wiley Online Library on [01/11/2023]. See the Terms and Conditions (https://onlinelibrary.wiley.com/terms-and-conditions) on Wiley Online Library for rules of use; OA articles are governed by the applicable Creative Commons License

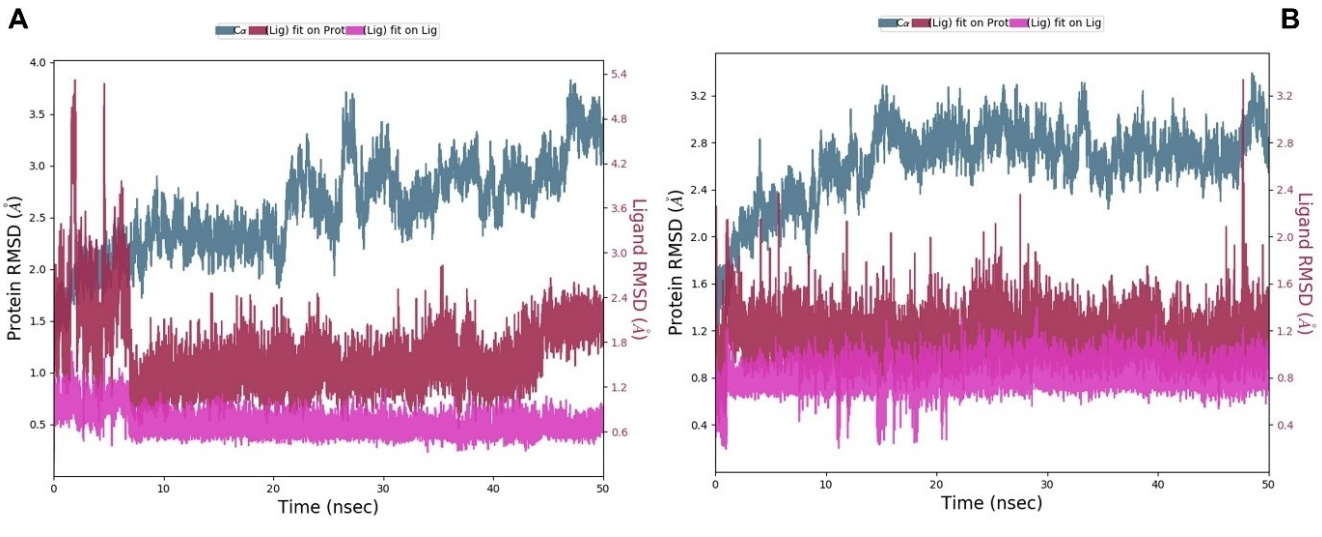


**Figure 9.** RMSD values of ligand atoms and protein Cα atoms of **TGFβ2-11** (A) and **TGFβ2-17** (B) complexes during simulation time. The left y-axis represents the Root Mean Square Deviation (RMSD) of Protein Cα (blue), while the right y-axis represents the RMSD of the ligand fit on the protein (red). The pink line represents the RMSD of the ligand, indicating its deviation from its reference conformation.

gen bonds, hydrophobic, ionic, and water bridges and summarized as shown in Figure 10. Stacked bar charts are relative along the coordinates. For example, a value of 0.7 indicates that certain interaction is maintained for 70% of the simulation time. Values higher than 1.0 are possible as some protein residues may interact with the ligand more than once in the same subtype.

Figure 10 demonstrated interaction fraction histograms of the ligand with each of the key residues of the protein during 50 nsec simulation time. In Figure 10, the hydrogen bond interactions were presented in green columns, the hydrophobic interactions were presented in purple columns and the water-bridged hydrogen bond interactions were presented in blue columns. According to Figure 10, the most abundant interactions have been observed, with Val-250 and His-328 during all the simulation time.

## MD Simulations on VEGFR2

For the VEGFR2 protein the complex of **VEGFR2-11** and **VEGFR2-15** were analyzed. The ligand-protein 2D key interactions with simulation times of **VEGFR2-11** and **VEGFR2-15** complexes were given in Figure 11.

As seen in Figure 11A, The carbonyl and nitrogen atoms of the hydrazide group of compound **11** formed hydrogen bond interactions with Asp-1046 (98% of sim.) and Glu-885 (99% of sim.) during all the simulation time. Furthermore, there is an intramolecular hydrogen bond interaction (77% of sim.) between hydrazide carbonyl and amide NH. Compound **11** interacted with Phe-1047 (49% of sim.) Phe-918 (10% of sim.) and His-1026 (47% of sim.) via pi-pi stacking interactions. In addition, the thiophene ring formed a pi-cationic interaction (65% of sim.) with Lys-868.

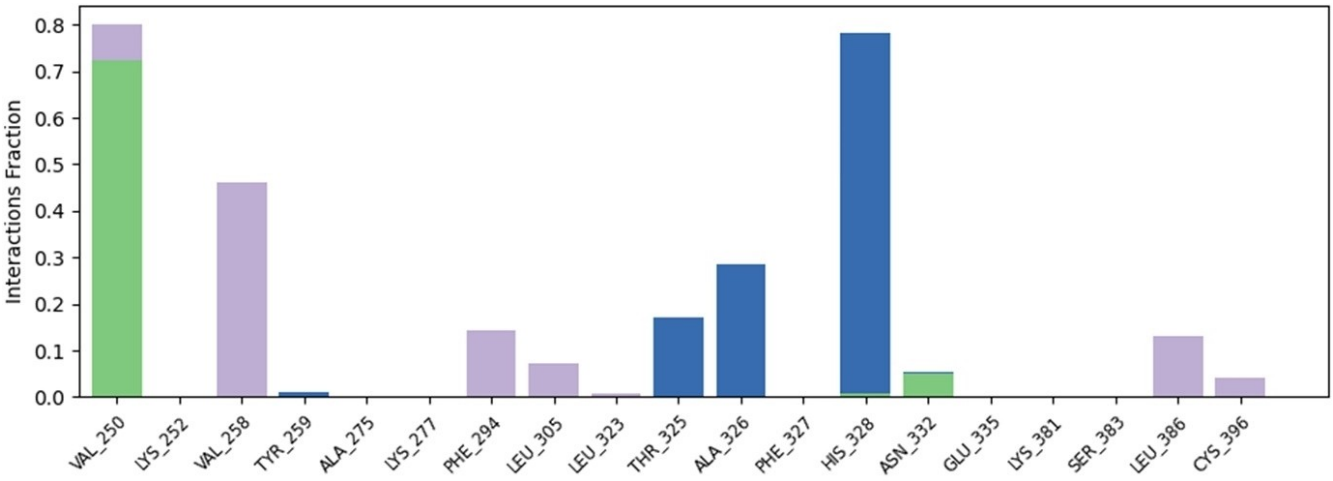


**Figure 10.** MD interaction fraction histograms of the **TGFβ2-17** complex.


© 2023 Wiley-VCH GmbH

23656549, 2023, 39, Downloaded from https://chemistry-europe.onlinelibrary.wiley.com/doi/10.1002/slct.202302448 by Bezm-I Alem Vakif University, Wiley Online Library on [01/11/2023]. See the Terms and Conditions (https://onlinelibrary.wiley.com/terms-and-conditions) on Wiley Online Library for rules of use; OA articles are governed by the applicable Creative Commons License

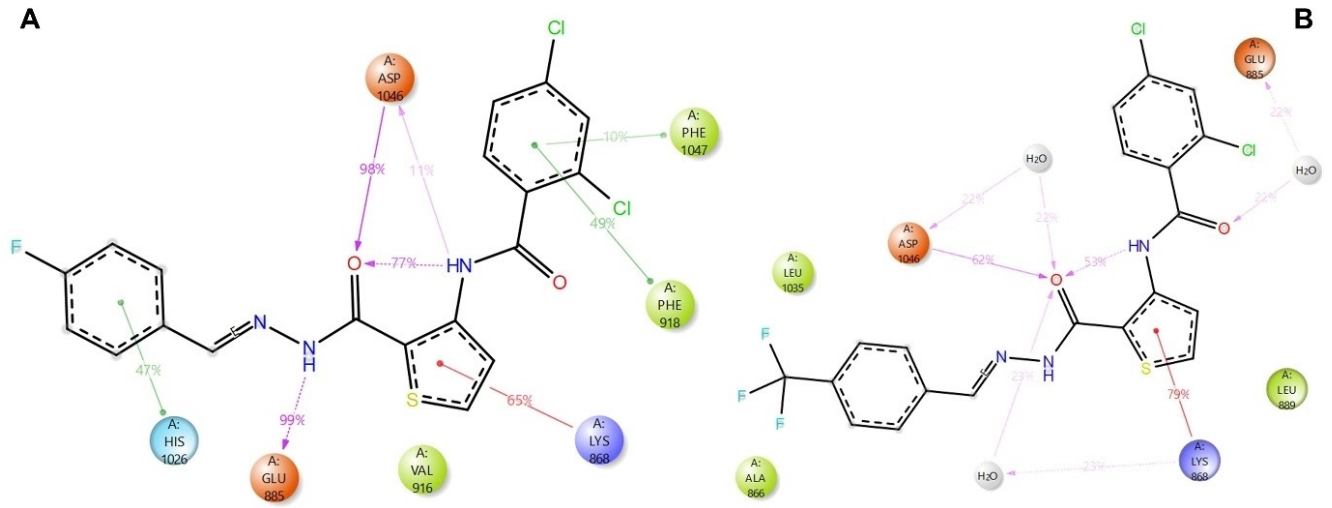


**Figure 11.** The MD ligand-protein 2D key interactions with % of simulation time of **VEGFR2-11** (A) and **VEGFR2-15** (B) complexes.

In Figure 11B, compound **15** formed three different water-bridged hydrogen bond interactions with Asp-1046 (22% of sim.), Glu-885 (22% of sim.) and Lys-868 (235 of sim.). The important interactions are the hydrogen bond interaction between Aps-1046 and carbonyl oxygen (62% of sim.) and intramolecular hydrogen bond interaction (53% of sim.). The intramolecular hydrogen bond is very important because this hydrogen bond kept the molecule rigidly and restricted the free rotation of the carbonyl group. Finally, thiophene ring formed pi-cationic interaction with Lys-868 during 79% of the simulation time.

As can be seen from Figure 12A, the **VEGFR2-11** complex was found as very stable complex because the average RMSD values of the ligand atoms and protein Cα atoms were found as 1.3 Å and 1.8 Å, respectively. In addition, as seen in Figure 12B, the **VEGFR2-15** is also stable. The average RMSD values of the ligand atoms and protein Cα atoms of the **VEGFR2-15** complex were found as 2.5 Å and 2 Å, respectively. According to the RMSD values, the **VEGFR2-11** complex is more stable than **VEGFR2-15**.

Figure 13 shows interaction fraction histograms of the ligand with each of the key residues of the protein during 50 nsec simulation time of **VEGFR2-11** complex.

In Figure 13, the hydrogen bond interactions were presented in green columns, the hydrophobic interactions were presented in purple columns and the water-bridged hydrogen bond interactions were presented in blue columns. According to Figure 13, the most abundant interactions have been observed, with Glu-885 and Asp-1046 during all the simulation time. In addition, Lys-868, Val-916, Phe-918, His-1026 and Phe-

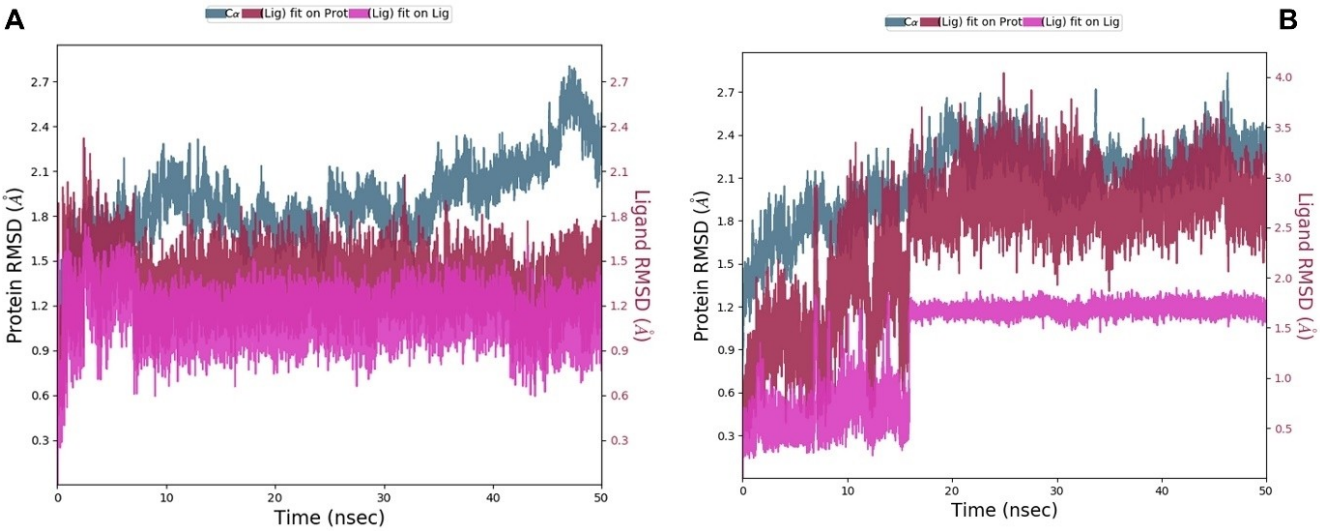


**Figure 12.** RMSD values of ligand atoms and protein Cα atoms of **VEGFR2-11** (A) and **VEGFR2-15** (B) complexes during simulation time. The left y-axis represents the Root Mean Square Deviation (RMSD) of Protein Cα (blue), while the right y-axis represents the RMSD of the ligand fit on the protein (red). The pink line represents the RMSD of the ligand, indicating its deviation from its reference conformation.


© 2023 Wiley-VCH GmbH

23656549, 2023, 39, Downloaded from https://chemistry-europe.onlinelibrary.wiley.com/doi/10.1002/slct.202302448 by Bezm-I Alem Vakif University, Wiley Online Library on [01/11/2023]. See the Terms and Conditions (https://onlinelibrary.wiley.com/terms-and-conditions) on Wiley Online Library for rules of use; OA articles are governed by the applicable Creative Commons License

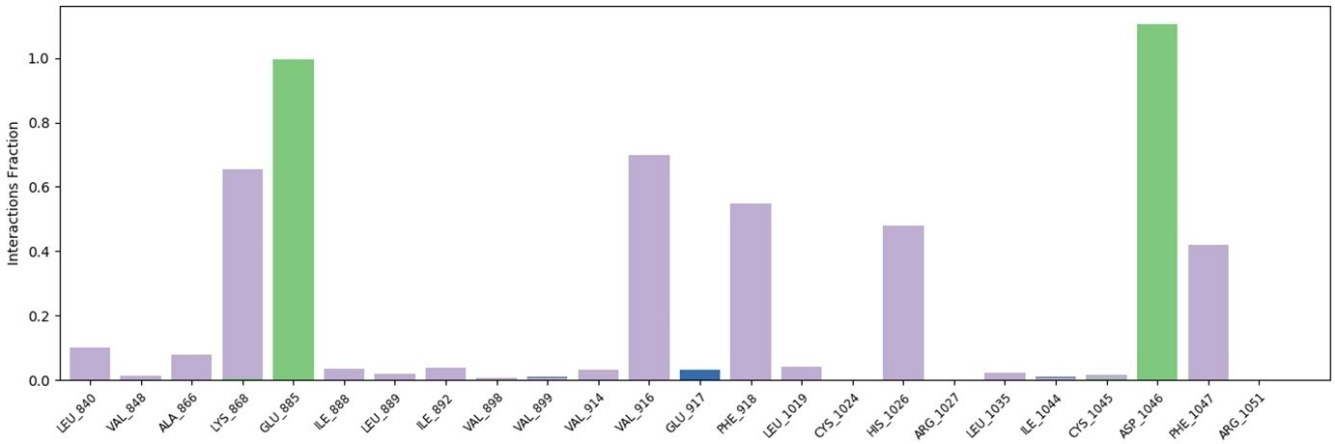


**Figure 13.** MD interaction fraction histograms of the **TGFβ2-17** complex.

1047 showed polar and apolar interaction during more than half of the simulation time.

## In Silico ADME Studies

To predict the physicochemical descriptors, pharmacokinetic properties, and drug-likeness of all the compounds ADME (absorption, distribution, metabolism, and excretion) studies were performed. In *in silico* ADME studies, predicted octanol/water partition coefficient, predicted aqueous solubility, predicted apparent Caco-2 cell permeability in nm/sec., predicted brain/blood partition coefficient, predicted apparent MDCK cell permeability in nm/sec., predicted human oral absorption on 0–100% scale, number of violations of Lipinski's rule of five, and number of violations of Jorgensen's rule of three parameters were determined and evaluated.[24] ADME prediction results of the target compounds were summarized in Table 3. There are generally two important descriptors for molecules to be considered a drug.[25] The first descriptor is Rule of five (RO5) which is a number of violations of Lipinski's rule of five[26] and the second one is Rule of three (RO3) which is number of violations of Jorgensen's rule of three.[27] For considering a molecule as a drug, the value of these two descriptors is expected to be zero but 3 of Lipinski's 5 rules and 2 of Jorgensen's 3 rules can be violated.[25,28]

According to the predicted ADME results, the most active compounds (**11, 15**, and **17**) showed better ADME properties compared to known drugs doxorubicin. Compounds **11, 15**, and **17** have moderate hydrogen bonding capabilities, potentially enabling interactions with biological systems.

Compounds **11, 15**, and **17** exhibit positive LogP values, suggesting they have a preference for partitioning into lipid-rich environments. Doxorubicin, with its negative LogP value, is more hydrophilic. Compounds **11, 15**, and **17** exhibit high predicted Caco-2 permeability values, suggesting efficient absorption through the gut-blood barrier. Gefitinib also has high permeability, while doxorubicin's permeability is comparatively lower. Compounds **11, 15**, and **17** exhibit high predicted MDCK permeability values, indicating efficient transport across cellular barriers. Gefitinib's permeability is lower, and doxorubicin's is substantially lower. All compounds show 100% predicted human oral absorption, indicating efficient absorption from the gastrointestinal tract. Gefitinib also displays high oral absorption, while doxorubicin used as intravenous and is not suitable for oral usage. Compounds **11, 15**, and **17** consistently show better or comparable ADME properties compared to doxorubicin. These compounds also generally outperform gefitinib, particularly in terms of Caco-2 permeability and MDCK

**Table 3.** ADME predictions results of the most active compounds and reference drugs.

| Parameters | **11** | **15** | **17** | Dox*. | Gef*. |
|---|---|---|---|---|---|
| MW[i] | 436.28 | 486.29 | 454.27 | 543.52 | 446.90 |
| Donor H bond[ii] | 1 | 1 | 1 | 5 | 1 |
| Accept H bond[iii] | 4 | 4 | 4 | 14 | 7 |
| QPLogpo/w[iv] | 5.93 | 6.69 | 6.11 | −0.52 | 4.27 |
| QPlogS[v] | −7.68 | −8.78 | −8.01 | −2.28 | −4.64 |
| QPPCaco[vi] | 1447 | 1457 | 1387 | 3 | 1121 |
| QPlogBB[vii] | −0.23 | −0.09 | −0.18 | −2.82 | 0.37 |
| QPPMDCK[viii] | 10000 | 10000 | 10000 | 1 | 2475 |
| % HOA[ix] | 100 | 100 | 100 | 0 | 100 |
| Rule of 5[x] | 1 | 1 | 1 | 3 | 0 |
| Rule of 3[xi] | 1 | 1 | 1 | 2 | 0 |

* *Dox.* = *Doxorubicin, Gef.* = *Gefitinib; **i)*** Molecular weight of the molecule 130–725 g/mol; ***ii)*** Estimated number of hydrogen bonds that would be donated by the solute to water molecules in an aqueous solution 0.0–6.0; ***iii)*** Estimated number of hydrogen bonds that would be accepted by the solute from water molecules in an aqueous solution 2.0–20.0; ***iv)*** Predicted octanol/water partition coefficient −2.0–6.5; ***v)*** Predicted aqueous solubility −6.5–0.5; ***vi)*** Predicted apparent Caco-2 cell permeability in nm/sec. Caco-2 cells are a model for the gut-blood barrier < 25 poor. > 500 great; vii) Predicted brain/blood partition coefficient −3.0–1.2; ***viii)*** Predicted apparent MDCK cell permeability in nm/sec. < 25 poor. > 500 great; ***ix)*** Predicted human oral absorption on 0–100% scale < 25% poor. > 80% high. The prediction is based on a quantitative multiple linear regression model; ***x)*** Number of violations of Lipinski's rule of five Max. is 4; ***xi)*** Number of violations of Jorgensen's rule of three Max. is 3.


© 2023 Wiley-VCH GmbH

23656549, 2023, 39, Downloaded from https://chemistry-europe.onlinelibrary.wiley.com/doi/10.1002/slct.202302448 by Bezm-I Alem Vakif University, Wiley Online Library on [01/11/2023]. See the Terms and Conditions (https://onlinelibrary.wiley.com/terms-and-conditions) on Wiley Online Library for rules of use; OA articles are governed by the applicable Creative Commons License

permeability. Compounds **11, 15**, and **17** each have one violation of Lipinski's and Jorgensen's rules, which is considered acceptable. Doxorubicin violates both rules to a greater extent, while gefitinib has no violations.

In conclusion, compounds **11, 15**, and **17** demonstrate favorable ADME characteristics, making them potentially promising candidates for anti-cancer drug development. They display improved properties in comparison to both doxorubicin and gefitinib across various parameters, including permeability, solubility, and absorption. These results suggest that compounds **11, 15**, and **17** could be more effective and better tolerated anti-cancer agents, paving the way for further preclinical and clinical investigations.

### Molecular Docking Validation Studies

The co-crystallized ligands of 5QIN (J2V) and 4ASE (AV9, Tivozanib) were re-docked at their actual crystal positions without changing their states or producing any conformers, thereby validating the molecular docking methods and protocols.[9] The original crystallographic conformation was superimposed with the co-crystallized ligand's docked pose, and the RMSDs were found to be 0.1981 Å for 5QIN and 0.2753 Å for 4ASE. Docking validation images are given in Figure 14.

The co-crystallized ligand is shown in green, and the re-docked ligand is shown as pink balls and stick modeling. RMSD (root-mean square deviation) values are often used to determine the quality of reproductive binding pose by molecular docking. The poses with RMSD less than 2 Å are often used as a criterion of the correct bound structure prediction while the value between 2–3 Å is acceptable.[29]

### Structure Activity Relationship

The structure-activity relationships of the synthesized compounds were evaluated according to the results of both *in vitro* and *in silico* biological activity studies. In *in vitro* cytotoxic activity studies, compounds **5, 11, 15**, and **17** were found to exhibit better cytotoxicity against HCT116 cells than gefitinib. When the functional groups were evaluated in the most active compounds, they were seen that there are 2-fluoro in compound **5**, 4-fluoro in compound **11**, 4-$CF_3$ in compound **15** and 2–6-difluoro in compound **17**. It appears that the fluorine atom or fluorinated side group must be carried in the ortho or para positions in the benzene ring for high biological activity. In compounds with fluorine or $CF_3$ group in meta, the activity is lower than ortho and para, but activity is still observed. The activity in the chlorinated and brominated derivatives is either very low or no appreciable. When the structure-activity relationships are evaluated according to molecular docking and dynamics studies, it is seen that the 2,4-dichlorobenzamide group is necessary for the activity because the chlorine atoms make halogen bond interactions with the amino acid residues in the active site of the enzyme. In addition, according to the MD simulations, the molecule remained in a constant geometry and bound to the active site of the enzyme with high affinity through the intramolecular hydrogen bond between the amide carbonyl and the hydrazide hydrogen. The fact that the 3-(2,4-dichlorobenzamido)-thiophene-2-carbohydrazide skeleton is in the V shape allows it to establish a good relationship with amino acid residues located in the V shape in the active site of the TGFβ2 enzyme. These interactions are also seen in detail from molecular docking and dynamics studies.

## Conclusions

In this study, eighteen novel arylidenehydrazide derivatives (compounds **4**–**21**) were synthesized starting from 3-amino-thiophene-2-carboxylic acid methyl ester. These compounds were then subjected to comprehensive evaluation to assess their potential as anti-cancer agents. The primary objectives included determining their cytotoxic effects against HCT116 (cancer) and HUVEC (normal) cell lines, understanding their molecular interactions with relevant proteins through molecular docking and dynamics studies, and assessing their drug-likeness and ADME properties using computational methods.

In the evaluation of both molecular docking and *in vitro* anti-cancer activity studies, it was observed that compounds

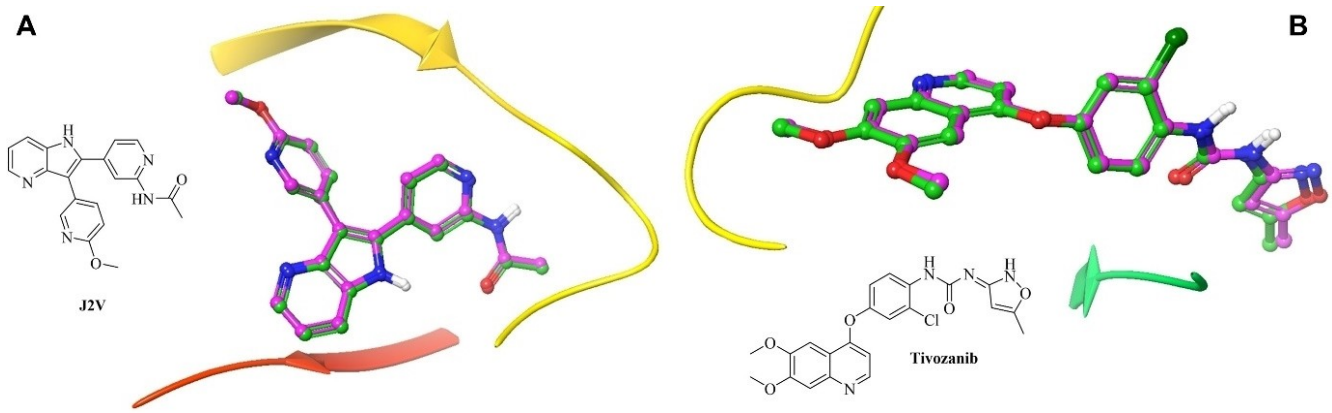


**Figure 14.** Docking validation images of J2 V on 5QIN (A) and tivozanib on 4ASE (B).


© 2023 Wiley-VCH GmbH

23656549, 2023, 39, Downloaded from https://chemistry-europe.onlinelibrary.wiley.com/doi/10.1002/slct.202302448 by Bezm-I Alem Vakif University, Wiley Online Library on [01/11/2023]. See the Terms and Conditions (https://onlinelibrary.wiley.com/terms-and-conditions) on Wiley Online Library for rules of use; OA articles are governed by the applicable Creative Commons License

**11, 15**, and **17** exhibited the highest levels of both selectivity and activity. These compounds demonstrated better anti-cancer effects when compared to the reference drugs, doxorubicin and gefitinib. Molecular dynamics (MD) simulations were employed to assess the stability of the ligand-protein complexes over time. Among the complexes, **TGFβ2-17** and **VEGFR2-11** demonstrated the highest stability, as indicated by the root mean square deviation (RMSD) values of the ligand atoms. The observed stability in these complexes holds significance, as stable interactions are more resistant to dissociation.

These findings underscore the potential superiority of compounds **11, 15**, and **17** over the reference drugs in terms of both selectivity and anti-cancer activity. The selectivity ratios reveal that these compounds are notably more effective at targeting cancer cells while minimizing the impact on normal cells when compared to both doxorubicin and gefitinib. This high selectivity, combined with *in vitro* and *in-silico* anti-cancer activity, positions compounds **11, 15**, and **17** as promising candidates for further development in anti-cancer therapy.

In conclusion, compound **11**′s potent anti-colon cancer effects, promising pathway inhibition, and superior attributes compared to existing drugs make it a compelling and promising candidate for further exploration and development in the field of colon cancer treatment. Its potential to address the limitations of current therapies and to offer a more effective and targeted approach makes it a promising potential candidate as an anti-cancer agent.

## Experimental Section

### Synthesis

The chemicals used in the synthesis were purchased from Sigma-Aldrich, Merck and 1Pluschem The chromatographic purifications were performed using a silica-gel column. Thin-layer chromatography (TLC) was used to monitor the experiments and column chromatography, and UV light. All the synthesized compounds were very well characterized by NMR ($^{1}$H, $^{19}$F, $^{13}$C-APT, HSQC, and HMBC) HRMS, and IR spectroscopic techniques. $^{1}$H-NMR, $^{13}$CAPT NMR, and $^{19}$F NMR spectra were recorded by Bruker Avance NEO NMR Spectrometer at 500, 125 and 471 MHz, respectively. Coupling constant values were given in Hertz (Hz). Chemical shifts were reported in δ (parts per million) units relative to the internal standard tetramethyl silane (δ = 0.00 ppm) and the peak splits were described as follows: s (singlet), d (doublet), t (triplet), q (quartet), m (multiplet), bs (broad singlet), dd (doublet of doublets) and dt (doublet of triplets). HRMS spectra were recorded using the ESI technique by Thermo Fischer Scientific Q Exactive™ Hybrid Quadrupole-Orbitrap™ Mass Spectrometer. The IR spectra were recorded by Bruker ALPHA II FT-IR Spectrometer and melting points were determined using STUART SMP 30 melting point apparatus.

### Synthesis of methyl 3-(2,4-dichlorobenzamido) thiophene-2-carboxylate (2)

A round-bottomed flask was charged with DCM (500 mL) and compound **1** (STM) (20 g, 127.24 mmol, 1 equiv.) was dissolved. $NaHCO_3$ (21.38 g, 254.47 mmol, 2 equiv.) and 2,4-dichlorobenzoyl chloride (33.31 g, 22.36 mL, 159 mmol, 1.25 equiv.) were added. The resulting mixture was stirred overnight at room temperature. After completion excess $NaHCO_3$ was filtered and the solution was washed with water (3 x 250 mL) and extracted with DCM (3 x 250 mL). All organic layers were combined, dried over $Na_2SO_4$ and filtered. The residue was adsorbed on silica gel and compound **2** was purified by silica gel column chromatography using an ethyl acetate-hexane mixture (1 : 4). (White solid, 42 g, 99.9% yield). **m.p.** 134–136 °C; **$^{1}$H NMR (500 MHz, $CDCl_3$) δ** 10.68 (s, 1H, NH), 8.17 (d, *J* = 5.5 Hz, 1H, thiophene SCH), 7.59 (d, *J* = 8.3 Hz, 1H, aromatic, benzene), 7.45 (d, *J* = 5.5 Hz, 1H, thiophene SCCH), 7.40 (d, *J* = 2.1 Hz, 1H, aromatic), 7.27 (dd, *J* = 8.3, 2.0 Hz, 1H, aromatic, 5$^{th}$ position of benzene), 3.80 (s, 3H, $CH_3O$); **$^{13}$C NMR (125 MHz, $CDCl_3$) δ** 164.63 (COO), 162.94 (CON), 143.94, 137.46, 133.23, 132.28, 131.85, 131.04, 130.52, 127.64, 122.55, 111.43, 52.10 ($CH_3O$); **HSQC NMR, $^{13}$C-$^{1}$H δ** 122.47–8.27 (thiophene SCH), 131.04–7.69, 131.73–7.45 (thiophene SCCH), 130.55–7.49, 127.61–7.37, 52.10-3.89 (methoxy); **FT-IR (cm$^{-1}$) $\nu_{max}$**: 3307 (NH), 3084 (C=C<u>H</u> stretch), 3024 (C=C<u>H</u> stretch), 2956 (C–H stretch), 1675 (COO), 1572 (CON), 1487 (C=C stretch), 1464 (C=C stretch), 1442 (C=C stretch), 1375 ($CH_3$ swing), 1339 (C–N stretch), 1139 (C–O stretch), 1102, 1081, 1054, 1005; **ESI-HRMS: m/z** Formula: $C_{13}H_9Cl_2NO_3S$, Calculated $[M+H]^+$: 329.97584, Found $[M+H]^+$: 329.97476.

### Synthesis of 2,4-dichloro-N-(2-(hydrazinecarbonyl)thiophen-3-yl)benzamide (3)

A round bottom flask was charged with ethanol (500 mL) and compound **2** (10 g, 30 mmol, 1 equiv.) was dissolved in. Hydrazine hydrate (7.4 mL, 80%, 151 mmol, 5 equiv.) and a catalytic amount of PTSA were added and stirred overnight under reflux conditions. After completion the reaction mixture was concentrated and cold until 0–5 °C. Diethyl ether was added to the cold mixture and stirred 30 minutes. The precipitated product was filtered and dried at rt. Compound **3** was obtained as white solid (30 g, %75 yield; Reaction was repeated 4 times). ***Compound 3:*** **m.p.** 213 – 215 °C; **$^{1}$H NMR (500 MHz, DMSO-$d_6$) δ** 12.58 (s, 1H, hydrazide NH), 9.09 (s, 1H, amide NH), 8.03 (d, *J* = 5.4 Hz, 2H, aromatic), 7.86–7.69 (m, 2H, aromatic), 7.59 (d, *J* = 8.1 Hz, 1H aromatic), 4.88 (s, 2H, hydrazide $NH_2$); **FT-IR (cm$^{-1}$) $\nu_{max}$**: 3315 (NH), 3246 (NH), 3207 (NH), 3079 (C=C<u>H</u> stretch), 1667 (COO), 1620 (CON), 1573 (C=C<u>H</u> stretch), 1554 (C=C<u>H</u> stretch), 1523 (C=C<u>H</u> stretch), 1474 (C=C<u>H</u> stretch), 1446, 1421, 1395, 1373, 1335 (C–N stretch), 1277, 1255, 1236, 1160, 1139, 1105, 1090, 1054, 996, 966, 938; **ESI-HRMS: m/z** Formula: $C_{12}H_9Cl_2N_3O_2S$, Calculated $[M-H]^+$: 327.97143, Found $[M-H]^+$: 327.97238.

### General Synthesis of Target Compounds (4–21)

A round bottom flask was charged with ethanol (50 mL) and hydrazid compound **3** (1.5 g, 4.54 mmol, 1 equiv.) was dissolved. Corresponding aldehyde (6.81 mmol, 1.5 equiv.) and catalytic amount of acetic acid were added and stirred six hours under reflux. After completion the reaction mixture was kept at room temperature for two days and product self-precipitated. The precipitated products were filtered and dried. As a result, target compounds were obtained as pure with yield from 80% to 99%.

***(E)-N-(2-(2-benzylidenehydrazine-1-carbonyl)thiophen-3-yl)-2,4-dichlorobenzamide (4):*** Starting from benzaldehyde and compound **3**. White solid, 1.52 g, 80% yield. **m.p.** 222–224 °C; **$^{1}$H NMR (500 MHz, DMSO-$d_6$) δ** 12.22 (s, 1H, hydrazide NH), 11.97 (s, 1H, amide NH), 8.21 (d, *J* = 5.5 Hz, 1H, aromatic), 8.16 (s, 1H, CH=N, imine), 8.07 (d, *J* = 5.6 Hz, 1H, aromatic), 7.89–7.72 (m, 4H, aromatic), 7.60 (dd, *J* = 8.3, 2.1 Hz, 1H, aromatic), 7.49 (dt, *J* = 13.8, 7.0 Hz, 3H, aromatic); **$^{13}$C NMR (125 MHz, DMSO) δ** 164.84 (hydrazide CO), 162.74 (amide CO), 145.55 (imine CH=N), 145.43, 136.49, 136.45, 134.78, 134.35, 131.77, 131.21, 130.71, 130.38, 129.46, 128.46,


© 2023 Wiley-VCH GmbH

23656549, 2023, 39, Downloaded from https://chemistry-europe.onlinelibrary.wiley.com/doi/10.1002/slct.202302448 by Bezm-I Alem Vakif University, Wiley Online Library on [01/11/2023]. See the Terms and Conditions (https://onlinelibrary.wiley.com/terms-and-conditions) on Wiley Online Library for rules of use; OA articles are governed by the applicable Creative Commons License

127.93, 121.01, 110.00; **HSQC NMR, $^{13}$C-$^{1}$H δ** 120.98–8.21, 145.60–8.16, 136.46–8.07, 127.97–7.83, 130.93–7.79, 128.44–7.60, 129.60–7.49; **FT-IR (cm$^{-1}$) $\nu_{max}$**: 3239 (NH), 3146 (C=CH stretch), 3102 (C=CH stretch), 2911 (C–H stretch), 2847 (C–H stretch), 1663 (CON), 1629 (CONN), 1556 (C=C stretch), 1508 (C=C stretch), 1453 (C=C stretch), 1307 (C–N stretch), 1260, 1223, 1158, **ESI-HRMS: m/z** Formula: $C_{19}H_{13}Cl_2N_3O_2S$, Calculated [M−H]$^+$: 416.00273, Found [M−H]$^+$: 416.00385.

***(E)-2,4-dichloro-N-(2-(2-(2-fluorobenzylidene)hydrazine-1-carbonyl)thiophen-3-yl)benzamide (5):*** Starting from 2-fluorobenzaldehyde and compound **3**. White solid, 1.58 g, 80% yield. **m.p.** 218–220 °C; **$^{1}$H NMR (500 MHz, DMSO-$d_6$) δ** 12.17 (s, 1H, hydrazide NH), 12.02 (s, 1H, amide NH), 8.35 (s, 1H, CH=N, imine), 8.20 (d, $J$=5.5 Hz, 1H, aromatic), 8.13–7.99 (m, 2H, aromatic), 7.76 (d, $J$=6.9 Hz, 1H, aromatic), 7.75 (s, 1H), 7.58 (dd, $J$=8.3, 2.1 Hz, 1H, aromatic), 7.48 (t, $J$=6.7 Hz, 1H, aromatic), 7.33 (t, $J$=7.7 Hz, 1H, aromatic), 7.28 (dd, $J$=10.9, 8.4 Hz, 1H); **$^{13}$C NMR (125 MHz, DMSO) δ** 164.85 (hydrazide CO), 162.70 (amide CO), 161.33 (d, $J$=250.5 Hz, *162.33, 160.33, CF aromatic*), 145.55 (CS), 138.17 (d, $J$=3.45 Hz, *138.19, 138.16*, (CH=N, imine)), 136.47 136.44, 134.68, 132.63 (d, $J$=8.5 Hz, *132.66, 132.59, CCCF aromatic*), 131.80, 131.21, 130.36, 128.40, 127.16, 125.49, 121.94 (d, $J$=9.8 Hz, *121.98, 121.90, CCCF aromatic*), 121.02, 116.55 (d, $J$=20.7 Hz, *116.63, 116.47, CCF aromatic*), 109.82; **HSQC NMR, $^{13}$C-$^{1}$H δ** 138.20–8.35, 121.00–8.20, 127.14-8.07, 136.37-8.04, 130.70–7.77, 128.40–7.57, 132.66-7.49, 125.49–7.33, 116.52–7.28; **$^{19}$F NMR (471 MHz, DMSO-$d_6$) δ** −120.31 (d, $J$=8.5 Hz); **FT-IR (cm$^{-1}$) $\nu_{max}$**: 3249 (NH), 3145 (NH), 3115(C=CH stretch), 3082 (C=CH stretch), 3027 (C=CH stretch), 2924 (C–H stretch), 2851 (C–H stretch), 1664 (C=ON), 1631 (C=ON), 1603 (CH=N), 1582 (C=CH stretch), 1557 (C=CH stretch), 1506 (C=CH stretch), 1482, 1454, 1401, 1372, 1353, 1330 (C–N stretch), 1298, 1280, 1263, 1234, 1204, 1188, 1161, 1140, 1126, 1092, 1052, 1030, 971; **ESI-HRMS: m/z** Formula: $C_{19}H_{12}Cl_2FN_3O_2S$, Calculated [M−H]$^+$: 433.99331, Found [M−H]$^+$: 433.99402.

***(E)-2,4-dichloro-N-(2-(2-(2-chlorobenzylidene)hydrazine-1-carbonyl)thiophen-3-yl)benzamide (6):*** Starting from 2-chlorobenzaldehyde and compound **3**. Yellow solid, 1.87 g, 91% yield. **m.p.** 206–208 °C; **$^{1}$H NMR (500 MHz, DMSO-$d_6$) δ** 12.16 (s, 1H, hydrazide NH), 12.08 (s, 1H, amide NH), 8.97 (s, 1H) 8.53 (s, 1H, CH=N, imine), 8.14 (dd, $J$=30.2, 16.0 Hz, 3H, aromatic), 8.03 (s, 1H, aromatic), 7.76 (d, $J$=10.6 Hz, 2H, aromatic), 7.62–7.37 (m, 5H, aromatic); **$^{13}$C NMR (125 MHz, DMSO) δ** 164.86 (hydrazide CO), 162.69 (amide CO), 158.72, 145.59 (CH=N, imine), 141.52, 136.47, 133.84, 133.49, 132.02, 131.81, 130.95, 130.46, 130.36, 128.58, 128.39, 128.16, 128.07, 127.64, 121.05; **FT-IR (cm$^{-1}$) $\nu_{max}$**: 3249 (NH), 3193 (NH), 3128 (C=CH stretch), 3111 (C–H stretch), 3082 (C=CH stretch), 2968 (C–H stretch), 1672 (hydrazide CO), 1623 (amide CO), 1581 (CH=N, imine), 1542 (C=C stretch), 1492(C=C stretch), 1448, 1425, 1396, 1345 (C–N stretch), 1318, 1264, 1234, 1160, 1131, 1100, 1048, 1030, 987, 952, 931, 896, 869 (C–Cl stretch), 838; **ESI-HRMS: m/z** Formula: $C_{19}H_{12}Cl_3N_3O_2S$, Calculated [M−H]$^+$: 449.96376, Found [M−H]$^+$: 449.96494.

***(E)-N-(2-(2-(2-bromobenzylidene)hydrazine-1-carbonyl)thiophen-3-yl)-2,4-dichlorobenzamide (7):*** Starting from 2-bromobenzaldehyde and compound **3**. Yellow solid, 2.23 g, 99% yield. **m.p**. 176.5–178.5 °C; **$^{1}$H NMR (500 MHz, DMSO-$d_6$) δ** 12.14 (s, 2H, hydrazide NH and amide NH), 8.54 (s, 1H, (CH=N, imine), 8.26–8.12 (m, 2H, aromatic), 8.08 (d, $J$=5.5 Hz, 1H, aromatic), 7.83 (d, $J$=2.0 Hz, 1H, aromatic), 7.79 (d, $J$=8.0 Hz, 1H), 7.73 (d, $J$=8.1 Hz, 1H), 7.62 (dd, $J$=8.2, 2.1 Hz, 1H), 7.58–7.47 (m, 2H), 7.40 (t, $J$=7.8 Hz, 1H); **$^{13}$C NMR (125 MHz, DMSO) δ** 164.90 (hydrazide CO), 162.71 (amide CO), 145.62 (CH=N, imine), 143.86, 136.49, 134.65, 133.72, 133.01, 132.25, 131.82, 131.19, 130.35, 128.66, 128.39, 128.00, 124.19, 121.06, 109.75; **FT-IR (cm$^{-1}$) $\nu_{max}$**: 3249 (NH), 3193 (C=CH stretch), 3130 (C=CH stretch), 3080 (C=CH stretch), 1672 (hydrazide CO), 1624 (amide CO), 1582 (CH=N, imine), 1547 (C=CH stretch), 1489 (C=CH stretch), 1453 (C=CH stretch), 1423, 1398, 1345 (C–N stretch), 1319, 1265, 1235, 1160, 1100, 1046, 1020, 930, 804, 763, 748, 712, 689 (C–Br stretch); **ESI-HRMS: m/z** Formula: $C_{19}H_{12}{}^{81}BrCl_2N_3O_2S$, Calculated [M−H]$^+$: 495.90730, Found [M−H]$^+$: 495.91202.

***(E)-2,4-dichloro-N-(2-(2-(3-fluorobenzylidene)hydrazine-1-carbonyl)thiophen-3-yl)benzamide (8):*** Starting from 3-fluorobenzaldehyde and compound **3**. Yellowish solid, 1.66 g, 84% yield. **m.p.** 231–233 °C; **$^{1}$H NMR (500 MHz, DMSO-$d_6$) δ** 12.17 (s, 1H, hydrazide NH), 12.04 (s, 1H, amide NH), 8.29–8.02 (m, 3H, CH=N, imine and aromatic), 7.85–7.68 (m, 2H), 7.57 (dq, $J$=38.3, 8.4, 7.5 Hz, 4H), 7.28 (t, $J$=8.7 Hz, 1H); **$^{13}$C NMR (125 MHz, DMSO) δ** 164.91 (hydrazide CO), 162.88 (d, $J$=243.76 Hz, *163.85, 161.91, CF aromatic*), 162.71 (amide CO), 145.55 (CS), 144 CH=N, imine), 136.85 (d, $J$=7.6 Hz, *136.88, 136.82, CCCF aromatic*), 136.52, 136.47, 134.70, 131.79, 131.50 (d, $J$=8.1 Hz, *131.53, 131.47, CCCF aromatic*), 131.22, 130.37, 128.42, 124.30, 121.03, 117.41 (d, $J$=21.4 Hz, *117.49, 117.32, CCF aromatic*), 113.87 (d, $J$=22.8 Hz, *113.96, 113.78, CCF aromatic*), 109.80; **HSQC NMR, $^{13}$C-$^{1}$H δ** 121.01-8.20, 144.18–8.13, 136.43–8.07, 130.73–7.77, 124.29–7.63, 113.84–7.61, 128.39–7.59, 131.50–7.52, 117.40–7.28; **$^{19}$F NMR (471 MHz, DMSO-$d_6$) δ** −112.19; **FT-IR (cm$^{-1}$) $\nu_{max}$**: 3242 (NH), 3149, (C=CH stretch) 3075 (C=CH stretch), 3026 (C=CH stretch), 1663 (hydrazide CO), 1631 (amide CO), 1557 (CH=N, imine), 1508 (C=C stretch), 1448 (C=C stretch), 1401, 1371, 1356, 1331 (C–N stretch), 1261, 1229, 1174, 1132, 1098, 1071, 1051, 965, 941, 894, 882, 861, 833, 768, 713, 676; **ESI-HRMS: m/z** Formula: $C_{19}H_{12}Cl_2FN_3O_2S$, Calculated [M−H]$^+$: 433.99331, Found [M−H]$^+$: 433.99432.

***(E)-2,4-dichloro-N-(2-(2-(3-chlorobenzylidene)hydrazine-1-carbonyl)thiophen-3-yl)benzamide (9):*** Starting from 3-chlorobenzaldehyde and compound **3**. Yellowish solid, 1.94 g, 94% yield. **m.p.** 216–218 °C; **$^{1}$H NMR (500 MHz, DMSO-$d_6$) δ** 12.17 (s, 1H, hydrazide NH), 12.05 (s, 1H, amide NH), 8.20 (d, $J$=5.6 Hz, 1H, HCS), 8.12 (s, 1H, CH=N, imine) 8.08 (m, 1H, aromatic), 7.92–7.69 (m, 4H, aromatic), 7.59 (d, $J$=8.4 Hz, 1H), 7.50 (d, $J$=6.9 Hz, 2H); **$^{13}$C NMR (125 MHz, DMSO) δ** 164.89 (hydrazide CO), 162.72 (amide CO), 145.57 (CS), 143.99 (CH=N, imine), 136.54, 136.47, 134.70, 134.22, 131.79, 131.27, 131.22, 130.38, 130.27, 128.43, 127.45, 126.34, 121.06 (HCS), 109.76. **HSQC NMR, $^{13}$C-$^{1}$H δ** 121.05–8.20 (HCS), 144.03–8.12 (CH=N, imine), 136.41–8.08, 127.20–7.81, 126.49–7.79, 130.69–7.78, 128.41–7.59, 130.7–7.49; **FT-IR (cm$^{-1}$) $\nu_{max}$**: 3237 (NH), 3145 (C=CH stretch), 3133 (C=CH stretch), 1664 (hydrazide CO), 1626 (amide CO), 1608 CH=N, imine, 1582 (C=C stretch), 1560 (C=C stretch), 1509 (C=C stretch), 1493 (C=C stretch), 1458 (C–H stretch), 1425, 1332 (C–N stretch), 1261, 1225, 1210, 1153, 1100, 1094, 1049, 1012, 988, 962, 950, 926, 899, 868 (C–Cl stretch), 832; **ESI-HRMS: m/z** Formula: $C_{19}H_{12}{}^{37}Cl_3N_3O_2S$, Calculated [M−H]$^+$: 451.95780, Found [M−H]$^+$: 451.96179.

***(E)-N-(2-(2-(3-bromobenzylidene)hydrazine-1-carbonyl)thiophen-3-yl)-2,4-dichlorobenzamide (10):*** Starting from 3-bromobenzaldehyde and compound **3**. White solid, 2.1 g, 93% yield. **m.p.** 220–222 °C; **$^{1}$H NMR (500 MHz, DMSO-$d_6$) δ** 12.16 (s, 1H, hydrazide NH), 12.06 (s, 1H, amide NH), 8.20 (d, $J$=5.4 Hz, 1H, HCS), 8.17–8.03 (m, 2H, aromatic and CH=N, imine), 7.96 (s, 1H, aromatic), 7.92–7.73 (m, 3H, aromatic), 7.62 (dd, $J$=17.1, 8.2 Hz, 2H), 7.45 (t, $J$=7.9 Hz, 1H); **$^{13}$C NMR (125 MHz, DMSO) δ** 164.88 (hydrazide CO), 162.74 (amide CO), 145.56 (CS), 143.96 (CH=N, imine), 136.77, 136.47, 134.72, 133.19, 131.78, 131.55, 131.22, 130.46, 130.39, 128.45, 122.73, 121.08, 109.75; **HSQC NMR, $^{13}$C-$^{1}$H δ** 121.08-8.20 (HCS), 144.01–8.12 (CH=N, imine), 136.42–8.09, 130.47–7.96, 126.68–7.84, 130.87–7.79, 133.21–7.63, 128.43–7.60, 131.60–7.45; **FT-IR (cm$^{-1}$) $\nu_{max}$**: 3266 (NH), 3230 (NH), 3088 (C=CH stretch), 1680 (hydrazide CO), 1639 (amide CO), 1619 (C=CH stretch), 1605 (C=C stretch), 1583 (C=C stretch), 1555 (C=C stretch), 1489, 1456, 1424, 1399, 1372, 1348, 1326 (C–N stretch), 1283, 1268, 1254, 1222, 1156, 1104, 1087, 1071, 1053, 995,


© 2023 Wiley-VCH GmbH

23656549, 2023, 39, Downloaded from https://chemistry-europe.onlinelibrary.wiley.com/doi/10.1002/slct.202302448 by Bezm-I Alem Vakif University, Wiley Online Library on [01/11/2023]. See the Terms and Conditions (https://onlinelibrary.wiley.com/terms-and-conditions) on Wiley Online Library for rules of use; OA articles are governed by the applicable Creative Commons License

967, 946, 904, 893, 865, 846 (C–Cl stretch), 829, 808, 775, 760, 735, 706, 680 (C–Br stretch), 671; **ESI-HRMS: m/z** Formula: $C_{19}H_{12}{}^{81}BrCl_2N_3O_2S$, Calculated $[M-H]^+$: 495.90730, Found $[M-H]^+$: 495.91205.

***(E)-2,4-dichloro-N-(2-(2-(4-fluorobenzylidene)hydrazine-1-carbonyl)thiophen-3-yl)benzamide (11):*** Starting from 4-fluorobenzaldehyde and compound **3**. Yellowish solid, 1.63 g, 82.5% yield. **m.p.** 254–256 °C; **$^1$H NMR (500 MHz, DMSO-$d_6$) δ** 12.20 (s, 1H, hydrazide NH), 11.97 (s, 1H) amide NH, 8.34 – 8.03 (m, 4H, aromatic), 7.84 (d, $J$ = 40.1 Hz, 3H, aromatic), 7.61 (s, 1H), 7.34 (s, 2H); **$^{13}$C NMR (125 MHz, DMSO) δ** 164.82 (hydrazide CO), 164.61 (amide CO), 162.73 (CF aromatic), 145.44 (CS), 144.43 (CH=N, imine), 136.45, 136.37, 134.77, 131.77, 130.99, 130.38, 130.11, 128.45, 121.04, 116.65, 116.48, 109.99; **HSQC NMR, $^{13}$C-$^1$H δ** 121.04–8.21 (HCS), 144.46–8.14 (CH=N, imine), 136.27–8.05, 130.19–7.87, 130.65–7.79, 128.49–7.60, 116.55–7.33; **$^{19}$F NMR (471 MHz, DMSO-$d_6$) δ** −110.01; **FT-IR (cm$^{-1}$) $\nu_{max}$**: 3237 (NH), 3180 (C=CH stretch), 3082 (C=CH stretch), 3014 (C=CH stretch), 1664 (hydrazide CO), 1626 (amide CO), 1608 (CH=N, imine), 1582 (C=CH stretch), 1560 (C=CH stretch), 1509 (C=CH stretch), 1493 (C=CH stretch), 1458, 1425, 1398, 1374, 1352, 1331 (C–N stretch), 1294, 1261, 1225, 1210, 1153, 1100, 1094, 1049, 1012, 988, 962, 950, 926, 899, 858 (C–Cl stretch), 832, 795, 772, 712, 691, 673, 657, 641; **ESI-HRMS: m/z** Formula: $C_{19}H_{12}Cl_2FN_3O_2S$, Calculated $[M-H]^+$: 433.99331, Found $[M-H]^+$: 433.99426.

***(E)-2,4-dichloro-N-(2-(2-(4-chlorobenzylidene)hydrazine-1-carbonyl)thiophen-3-yl)benzamide (12):*** Starting from 4-chlorobenzaldehyde and compound **3**. Yellowish solid, 1.99 g, 96.5% yield. **m.p.** 248–250 °C; **$^1$H NMR (500 MHz, DMSO-$d_6$) δ** 12.18 (s, 1H, hydrazide NH), 12.00 (s, 1H, amide NH), 8.36–8.00 (m, 3H, aromatic), 8.00–7.69 (m, 4H, aromatic), 7.72–7.37 (m, 3H); **$^{13}$C NMR (125 MHz, DMSO) δ** 164.84 (hydrazide CO), 162.71 (amide CO), 161.07, 145.49 (CS), 144.26 (CH=N, imine), 136.46, 136.39, 135.18, 134.72, 133.27, 131.79, 131.22, 130.45, 129.51, 128.43, 121.05, 109.88; **FT-IR (cm$^{-1}$) $\nu_{max}$**: 3238 (NH), 3148 (C=CH stretch), 3074 (C=CH stretch), 3022 (C=CH stretch), 1665 (hydrazide CO), 1628 (amide CO), 1601 (CH=N, imine), 1561 (C=C stretch), 1506 (C=C stretch), 1485 (C=C stretch), 1455, 1401, 1372, 1353, 1331 (C–N stretch), 1300, 1260, 1223, 1160, 1136, 1096, 1050, 1009, 954, 929, 897, 869 (C–Cl stretch), 825, 803, 772, 739, 715, 680, 640, 577, 531, 513, 459, 443, 417; **ESI-HRMS: m/z** Formula: $C_{19}H_{12}Cl_3N_3O_2S$, Calculated $[M-H]^+$: 449.96376, Found $[M-H]^+$: 449.96490.

***(E)-N-(2-(2-(4-bromobenzylidene)hydrazine-1-carbonyl)thiophen-3-yl)-2,4-dichlorobenzamide (13):*** Starting from 4-bromobenzaldehyde and compound **3**. Yellowish solid, 2.17 g, 96% yield. **m.p.** 256–258 °C; **$^1$H NMR (500 MHz, DMSO-$d_6$) δ** 12.16 (s, 1H, hydrazide NH), 12.00 (s, 1H, amide NH), 8.21 (s, 1H, HCS), 8.13 (s, 1H, CH=N, imine), 8.07 (d, $J$ = 5.6 Hz, 1H), 7.79 (dd, $J$ = 19.2, 10.2 Hz, 3H), 7.70 (d, $J$ = 8.3 Hz, 3H), 7.61 (d, $J$ = 8.3 Hz, 1H); **$^{13}$C NMR (125 MHz, DMSO) δ** 164.86 (hydrazide CO), 162.76 (amide CO), 145.49 (CS), 144.45 (CH=N, imine), 136.47, 134.77, 133.63, 132.49, 131.76, 131.23, 130.40, 129.76, 128.48, 124.02, 121.08, 109.93; **HSQC NMR, $^{13}$C-$^1$H δ** 121.04–8.21 (HCS), 144.50–8.12 (CH=N, imine), 136.41–8.07, 130.41–7.82, 129.90–7.77, 129.64–7.71, 132.49–7.70, 131.60–7.62, 128.51–7.61; **FT-IR (cm$^{-1}$) $\nu_{max}$**: 3228 (NH), 3188 (C=CH stretch), 3147 (C=CH stretch), 3098 (C=CH stretch), 3075 (C=CH stretch), 3022 (C=CH stretch), 1666 (hydrazide CO), 1628 amide NH, 1597 (CH=N, imine), 1563 (C=C stretch), 1505 (C=C stretch), 1483 (C=C stretch), 1456, 1402, 1373, 1355, 1332 (C–N stretch), 1299, 1261, 1223, 1159, 1136, 1098, 1064, 1004, 953, 929, 896, 871, 837 (C–Cl stretch), 814, 771, 733, 716, 678; **ESI-HRMS: m/z** Formula: $C_{19}H_{12}{}^{81}Br^{37}Cl_2N_3O_2S$, Calculated $[M-H]^+$: 497.90810, Found $[M-H]^+$: 497.90810.

***(E)-2,4-dichloro-N-(2-(2-(3-(trifluoromethyl)benzylidene)hydrazine-1-carbonyl)thiophen-3-yl)benzamide (14):*** Starting from 3-trifluoromethylbenzaldehyde and compound **3**. White solid, 1.955 g, 88.5% yield. **m.p.** 234–236 °C; **$^1$H NMR (500 MHz, DMSO-$d_6$) δ** 12.15 (s, 2H hydrazide NH and amide NH), 8.24 (s, 1H, CH=N, imine), 8.19–8.06 (m, 4H, aromatic), 7.82 (d, $J$ = 2.0 Hz, 1H), 7.80 (d, $J$ = 4.1 Hz, 1H), 7.78 (s, 1H), 7.74 (t, $J$ = 7.9 Hz, 1H), 7.62 (dd, $J$ = 8.3, 2.0 Hz, 1H); **$^{13}$CNMR (125 MHz, DMSO) δ** 164.96 (hydrazide CO), 162.79 (amide CO), 145.61 (CS), 143.95 (CH=N, imine), 136.49, 135.54, 134.73, 131.77, 131.23, 130.64, 130.39, 128.48, 124.93 (q, $J$ = 3.5 Hz, *126.96, 126.94, 126.91, 126.89, CCF$_3$ aromatic*), 124.52, 124.40 (q, $J$ = 272 Hz, *127.69, 125.53, 123.36, 121.23, CF$_3$*), 121.12, 109.72; **HSQC NMR, $^{13}$C-$^1$H δ** 143.99–8.24 (CH=N, imine), 121.13–8.21 (HCS),, 131.32–8.15, 124.54–8.13, 136.44–8.10, 130.41–7.82, 126.94–7.81, 131.24–7.79, 130.68–7.74, 128.46–7.62; **$^{19}$F NMR (471 MHz, DMSO-$d_6$) δ** −61.37 ($CF_3$); **FT-IR (cm$^{-1}$) $\nu_{max}$**: 3245 (NH), 3181 (C=CH stretch), 3127 (C=CH stretch), 3093 (C=CH stretch), 1672 (hydrazide CO), 1618 (amide CO), 1580 (CH=N, imine), 1545 (C=C stretch), 1485 (C=C stretch), 1440 (C=C stretch), 1401, 1318 (C–N stretch), 1263, 1213, 1173 ($CF_3$ stretch), 1112, 1065, 975, 950, 900, 845 (C–Cl stretch), 804, 760, 715, 687, 651, 612, 583, 557, 512, 453; **ESI-HRMS: m/z** Formula: $C_{20}H_{12}Cl_2F_3N_3O_2S$, Calculated $[M-H]^+$: 483.99011, Found $[M-H]^+$: 483.99121.

***(E)-2,4-dichloro-N-(2-(2-(4-(trifluoromethyl)benzylidene)hydrazine-1-carbonyl)thiophen-3-yl)benzamide (15):*** Starting from 4-trifluoromethylbenzaldehyde and compound **3**. Yellowish solid, 1.88 g, 85% yield. **m.p.** 236–238 °C; **$^1$H NMR (500 MHz, DMSO-$d_6$) δ** 12.14 (s, 1H, hydrazide NH), 12.13 (s, 1H, amide NH), 8.21 (s, 2H CH=N, imine and aromatic), 8.01 (d, $J$ = 8.1 Hz, 2H), 7.83 (d, $J$ = 8.0 Hz, 2H), 7.81–7.74 (m, 3H), 7.60 (dd, $J$ = 8.3, 2.1 Hz, 1H); **$^{13}$C NMR (125 MHz, DMSO) δ** 165.00 (hydrazide CO), 162.75 (amide CO), 145.61 (CS), 143.87 (CH=N, imine), 138.29, 136.53, 136.48, 134.69, 131.78, 131.23, 130.38, 130.11, 128.45,, 126.31, 124.49 (q, $J$ = 272 Hz, *127.75, 125.59, 123.42, 121.26, CF$_3$*), 121.10, 109.79; **HSQC NMR, $^{13}$C-$^1$H δ** 143.91–8.21 (CH=N, imine), 121.09–8.21 (HCS), 136.50–8.07, 128.47–8.01, 126.31–7.83, 130.55–7.80, 128.46–7.60; **$^{19}$F NMR (471 MHz, DMSO-$d_6$) δ** −61.24; **FT-IR (cm$^{-1}$) $\nu_{max}$**: 3241 (NH), 3147 (C=CH stretch), 3075 (C=CH stretch), 3023 (C=CH stretch), 1666 (hydrazide CO), 1628 (amide CO), 1596 (CH=N, imine), 1561 (C=C stretch), 1499 (C=C stretch), 1457 (C=C stretch), 1402, 1374, 1359, 1318, 1303, 1262, 1229, 1157 ($CF_3$ stretch), 1127 ($CF_3$ stretch), 1099, 1061, 1010, 964, 932, 896, 873, 834 ($CF_3$ stretch), 808, 770, 718, 678; **ESI-HRMS: m/z** Formula: $C_{20}H_{12}Cl_2F_3N_3O_2S$, Calculated $[M-H]^+$: 483.99011, Found $[M-H]^+$: 483.99109.

***(E)-N-(2-(2-(3,5-bis(trifluoromethyl)benzylidene)hydrazine-1-carbonyl)thiophen-3-yl)-2,4-dichlorobenzamide (16):*** Starting from 3,5-bis-trifluoromethylbenzaldehyde and compound **3**. White solid, 2.09 g, 83% yield. **m.p.** 251–253 °C; **$^1$H NMR (500 MHz, DMSO-$d_6$) δ** 12.32 (s, 1H, hydrazide NH), 12.09 (s, 1H amide NH), 8.45 (s, 1H, HCS), 8.29 (s, 1H, CH=N, imine), 8.24–8.04 (m, 2H), 7.81 (d, $J$ = 2.0 Hz, 1H), 7.78 (d, $J$ = 8.2 Hz, 1H), 7.61 (dd, $J$ = 8.2, 2.1 Hz, 1H); **$^{13}$C NMR (125 MHz, DMSO) δ** 164.99 (hydrazide CO), 162.79 (amide CO), 145.80 (CS), 142.32 (CH=N, imine), 137.17, 136.50, 136.30, 134.63, 131.78, 131.51, 131.24, 130.98, 130.39, 128.45, 127.96 (HCS), 123.51 (q, $J$ = 272.9 Hz, *126.86, 124.69, 122.52, 121.24, CF$_3$*), 123.44, 120.35, 109.34; **HSQC NMR, $^{13}$C-$^1$H δ** 127.94–8.45 (HCS), 142.37–8.30 (CH=N, imine), 121.22–8.20, 123.46–8.16, 136.27–8.13, 130.41–7.81, 131.05–7.80, 128.41–7.78, 128.44–7.61; **$^{19}$F NMR (471 MHz, DMSO-$d_6$) δ** −61.60; **FT-IR (cm$^{-1}$) $\nu_{max}$**: 3215 (NH), 3123 (C=CH stretch), 3089 (C=CH stretch), 3018 (C=CH stretch), 1673 (hydrazide CO), 1627 (amide CO), 1619 (CH=N, imine), 1548 (C=C stretch), 1488 (C=C stretch), 1451 (C=C stretch), 1425, 1403, 1380, 1327, 1271, 1180 ($CF_3$ stretch), 1127 ($CF_3$ stretch), 1102 ($CF_3$ stretch), 1054, 990, 949, 889, 841 (C–Cl stretch), 810, 764, 717; **ESI-HRMS: m/z** Formula: $C_{21}H_{11}Cl_2F_6N_3O_2S$, Calculated $[M-H]^+$: 551.97750, Found $[M-H]^+$: 551.97894.


© 2023 Wiley-VCH GmbH

23656549, 2023, 39, Downloaded from https://chemistry-europe.onlinelibrary.wiley.com/doi/10.1002/slct.202302448 by Bezm-I Alem Vakif University, Wiley Online Library on [01/11/2023]. See the Terms and Conditions (https://onlinelibrary.wiley.com/terms-and-conditions) on Wiley Online Library for rules of use; OA articles are governed by the applicable Creative Commons License

***(E)-2,4-dichloro-N-(2-(2-(2,6-difluorobenzylidene)hydrazine-1-carbonyl)thiophen-3-yl)benzamide (17):*** Starting from 2,6-difluorobenzaldehyde and compound **3**. White solid, 1.81 g, 88% yield. **m.p.** 209–211 °C; **$^1$H NMR (500 MHz, DMSO-$d_6$) δ** 12.11 (s, 1H, hydrazide NH), 12.00 (s, 1H amide NH), 8.31 (s, 1H, CH=N, imine), 8.24–8.13 (m, 1H, HCS), 8.06 (d, *J*=5.6 Hz, 1H, aromatic), 7.82 (d, *J*=2.0 Hz, 1H, aromatic), 7.79 (d, *J*=8.2 Hz, 1H), 7.62 (dd, *J*=8.3, 2.1 Hz, 1H), 7.55 (td, *J*=8.3, 4.0 Hz, 1H, aromatic), 7.24 (t, *J*=9.0 Hz, 2H); **$^{13}$C NMR (125 MHz, DMSO) δ** 164.86 (hydrazide CO), 162.76 (amide CO), 160.64 (d, *J*=255.2 Hz, *161.67, 159.65, CF aromatic*), 160.60 (d, *J*=255.2 Hz, *161.63, 159.60, CF aromatic*), 145.45 (CS), 136.70, 136.46, 135.34 (CH=N, imine), 134.76, 132.72, 131.76, 131.21, 130.39, 128.48, 120.84, 112.95, 112.76, 110.15; **HSQC NMR, $^{13}$C-$^1$H δ** 135.36-8.31 (CH=N, imine), 120.84–8.18 (HCS), 136.67–8.06, 130.40–7.82, 131.24–7.79, 128.46–7.62, 132.74–7.55, 112.86–7.24; **$^{19}$F NMR (471 MHz, DMSO-$d_6$) δ** −111.73; **FT-IR (cm$^{-1}$) $\nu_{max}$**: 3269 (NH), 3144 (C=CH stretch), 3098 (C=CH stretch), 3029 (C=CH stretch), 1680 (hydrazide CO), 1663 (amide CO), 1632 (CH=N, imine), 1604 (C=C stretch), 1581 (C=C stretch), 1549 (C=C stretch), 1503 (C=C stretch), 1475, 1461, 1404, 1376, 1327, 1294, 1256, 1236, 1221, 1162, 1140, 1127, 1099, 1051, 1006, 964, 923, 898, 874, 843 (C–Cl stretch), 807, 784, 767, 717, 697, 678, 644, 586, 556, 538; **ESI-HRMS: m/z** Formula: $C_{19}H_{11}Cl_2F_2N_3O_2S$, Calculated [M−H]$^+$: 451.98388, Found [M−H]$^+$: 451.98489.

***(E)-2,4-dichloro-N-(2-(2-(2,3-dichlorobenzylidene)hydrazine-1-carbonyl)thiophen-3-yl)benzamide (18):*** Starting from 2,3-dichlorobenzaldehyde and compound **3**. White solid, 2.05 g, 93% yield. **m.p.** 247–249 °C; **$^1$H NMR (500 MHz, DMSO-$d_6$) δ** 12.16 (s, 1H, hydrazide NH), 12.10 (s, 1H, amide NH), 8.57 (s, 1H, CH=N, imine), 8.20 (d, *J*=5.5 Hz, 1H, aromatic), 8.12 (d, *J*=7.9 Hz, 1H, aromatic), 8.06 (d, *J*=5.6 Hz, 1H, aromatic), 7.82 (d, *J*=2.0 Hz, 1H, aromatic), 7.79 (d, *J*=8.3 Hz, 1H, aromatic), 7.75–7.70 (m, 1H, aromatic), 7.61 (dd, *J*=8.3, 2.1 Hz, 1H, aromatic), 7.51 (t, *J*=8.0 Hz, 1H); **$^{13}$C NMR (125 MHz, DMSO) δ** 164.89 (hydrazide CO), 162.77 (amide CO), 145.66 (CS), 141.41 (CH=N, imine), 136.62, 136.49, 134.68, 134.02, 133.04, 132.17, 131.78, 131.68, 131.22, 130.40, 129.08, 128.47, 126.21, 121.09, 109.64; **HSQC NMR, $^{13}$C-$^1$H δ** 141.44–8.57 (CH=N, imine), 121.09–8.20 (HCS), 126.19–8.11, 136.57–8.06, 130.40–7.82, 131.17–7.79, 132.21–7.72, 128.49–7.61, 129.09–7.51; **FT-IR (cm$^{-1}$) $\nu_{max}$**: 3261 (NH), 3080 (C=CH stretch), 3026 (C=CH stretch), 1687 (hydrazide CO), 1659 (amide CO) 1628 (CH=N, imine), 1579 (C=C stretch), 1555 (C=C stretch), 1502 (C=C stretch), 1453 (C=C stretch), 1399, 1372, 1347, 1321, 1259, 1189, 1161, 1142, 1103, 1044, 973, 934, 901, 858 (C–Cl stretch), 830, 807, 778; **ESI-HRMS: m/z** Formula: $C_{19}H_{11}{}^{37}Cl_4N_3O_2S$, Calculated [M−H]$^+$: 485.93730, Found [M−H]$^+$: 485.92310.

***(E)-2,4-dichloro-N-(2-(2-(2,4-dichlorobenzylidene)hydrazine-1-carbonyl)thiophen-3-yl)benzamide (19):*** Starting from 2,4-dichlorobenzaldehyde and compound **3**. Cream color solid, 2.05 g, 93% yield. **m.p**. 248.5–250.5 °C; **$^1$H NMR (500 MHz, DMSO-$d_6$) δ** 12.17 (s, 1H, hydrazide NH), 12.09 (s, 1H amide NH), 8.58 (s, 1H CH=N, imine), 8.20 (d, *J*=5.5 Hz, 1H, aromatic), 8.12 (d, *J*=7.8 Hz, 1H, aromatic), 8.07 (d, *J*=5.6 Hz, 1H, aromatic), 7.83 (d, *J*=2.0 Hz, 1H, aromatic), 7.79 (d, *J*=8.2 Hz, 1H), 7.76–7.71 (m, 1H), 7.62 (dd, *J*=8.3, 2.0 Hz, 1H), 7.52 (t, *J*=8.1 Hz, 1H); **$^{13}$C NMR (125 MHz, DMSO) δ** 164.90 (hydrazide CO), 162.79 (amide CO), 145.67 (CS), 141.44 (CH=N, imine), 136.66, 136.49, 134.70, 134.04, 133.05, 132.20, 131.77, 131.69, 131.22, 130.40, 129.12, 128.49, 126.23, 121.10, 109.64; **HSQC NMR, $^{13}$C-$^1$H δ** 141.47–8.58 (CH=N, imine), 121.11–8.20 (HCS), 126.23–8.12, 136.64–8.07, 130.42–7.82, 131.26–7.79, 132.24–7.74, 128.47–7.62, 129.12–7.52; **FT-IR (cm$^{-1}$) $\nu_{max}$**: 3260 (NH), 3145 (C=CH stretch), 3080 (C=CH stretch), 3026 (C=CH stretch), 1687 (hydrazide CO), 1659 (amide CO), 1627 (CH=N, imine), 1554 (C=C stretch), 1502 (C=C stretch), 1453 (C=C stretch), 1399, 1372, 1161, 1142, 1103, 1044, 973, 934, 901, 858 (C–Cl stretch), 830, 807, 778, 755; **ESI-HRMS: m/z** Formula: $C_{19}H_{11}{}^{37}Cl_4N_3O_2S$, Calculated [M+H]$^+$: 487.95300, Found [M+H]$^+$: 487.93643.

***(E)-2,4-dichloro-N-(2-(2-(2-chloro-6-fluorobenzylidene)hydrazine-1-carbonyl)thiophen-3-yl)benzamide (20):*** Starting from 2-chloro-6-fluorobenzaldehyde and compound **3**. Yellowish solid, 1.74 g, 87.5% yield. **m.p.** 195–197 °C**; $^1$H NMR (500 MHz, DMSO-$d_6$) δ** 12.09 (s, 2H, hydrazide NH and amide NH), 8.42 (s, 1H, CH=N, imine), 8.22–8.13 (m, 1H, aromatic), 8.10–8.00 (m, 1H, aromatic), 7.82 (d, *J*=2.0 Hz, 1H, aromatic), 7.79 (d, *J*=8.3 Hz, 1H), 7.62 (dd, *J*=8.3, 2.1 Hz, 1H), 7.52 (q, *J*=7.4 Hz, 1H), 7.45 (d, *J*=8.0 Hz, 1H), 7.39 (d, *J*=9.7 Hz, 1H); **$^{13}$C NMR (125 MHz, DMSO) δ** 164.92 (hydrazide CO), 162.78 (amide CO), 160.32 (d, *J*=272 Hz, *161.35, 159.29, CF*) 145.46 (CS), 138.29 (CH=N, imine), 136.75, 136.46, 134.76, 134.61, 132.46, 131.76, 131.21, 130.38, 128.48, 126.60, 120.82, 116.27, 116.10, 110.07; **HSQC NMR, $^{13}$C-$^1$H δ** 138.33–8.42 (CH=N, imine), 120.84–8.17 (HCS), 136.69–8.04, 130.40–7.82, 131.23–7.79, 128.44–7.79, 128.46–7.62, 132.48–7.52, 126.58–7.45, 116.17–7.38; **$^{19}$F NMR (471 MHz, DMSO-$d_6$) δ**−108.62; **FT-IR (cm$^{-1}$) $\nu_{max}$**: 3249 (NH), 3144 (C=CH stretch), 3108 (C=CH stretch), 1669 (hydrazide CO), 1622 (amide CO), 1583 (CH=N, imine), 1537 (C=C stretch), 1493 (C=C stretch), 1452 (C=C stretch), 1433, 1396, 1351, 1319, 1278, 1257, 1225, 1184, 1150, 1099, 1050, 957, 931, 895, 895, 869, 841 (C–Cl stretch), 804, 781, 768, 746, 721; **ESI-HRMS: m/z** Formula: $C_{19}H_{11}{}^{37}Cl_3FN_3O_2S$, Calculated [M−H]$^+$: 469.96690, Found [M−H]$^+$: 469.95230.

***(E)-N-(2-(2-(5-bromo-2-hydroxybenzylidene)hydrazine-1-carbonyl)thiophen-3-yl)-2,4-dichlorobenzamide (21):*** Starting from 5-bromo-2-hydroxybenzaldehyde and compound **3**. Yellow solid, 2.07 g, 89% yield. **m.p.** 241–243 °C; **$^1$H NMR (500 MHz, DMSO-$d_6$) δ** 12.20 (s, 1H, hydrazide NH), 11.96 (s, 1H, amide NH), 10.51 (s, 1H, OH), 8.42 (s, 1H) CH=N, imine, 8.20 (d, *J*=5.4 Hz, 1H, aromatic), 8.13 (d, *J*=5.6 Hz, 1H, aromatic), 8.00 (s, 1H), 7.85–7.81 (m, 1H, aromatic), 7.79 (d, *J*=8.3 Hz, 1H, aromatic), 7.62 (dd, *J*=8.3, 2.0 Hz, 1H, aromatic), 7.43 (dd, *J*=8.8, 2.6 Hz, 1H, aromatic), 6.90 (d, *J*=8.7 Hz, 1H, aromatic); **$^{13}$C NMR (125 MHz, DMSO) δ** 164.66 (hydrazide CO), 162.76 (amide CO), 156.39 (C–O), 145.46 (CS), 140.62 (CH=N, imine), 136.46, 136.35, 134.77, 134.29, 131.77, 131.22, 130.39, 128.48, 122.97, 121.09 (HCS), 119.07, 111.34, 109.79; **HSQC NMR, $^{13}$C-$^1$H δ** 140.64–8.42 (CH=N, imine), 121.09–8.20 (HCS), 136.30–8.13, 128.56–8.00, 130.40–7.82, 131.23–7.79, 128.46–7.62, 134.31–7.43, 119.10–6.90; **FT-IR (cm$^{-1}$) $\nu_{max}$**: 3296 (NH), 3236 (NH), 3100 (C=CH stretch), 3053 (C=CH stretch), 3026 (C=CH stretch), 1664 (hydrazide CO), 1609 (amide CO), 1559 (CH=N, imine), 1478(C=C stretch), 1437 (C=C stretch), 1402, 1371, 1331, 1259, 1236, 1178, 1159, 1135, 1099, 1082, 1047, 957, 897, 872, 850 (C–Cl stretch), 823, 812, 802, 756; **ESI-HRMS: m/z** Formula: $C_{19}H_{12}{}^{81}BrCl_2N_3O_3S$, Calculated [M−H]$^+$: 511.90220, Found [M−H]$^+$: 511.90668.

## In vitro Anti-Cancer Activity Studies

### *Cell Culture*

In this study, the human umbilical vein endothelial cell (HUVEC) and human colon cancer cell (HCT-116) lines were used. The cells were grown in DMEM/F12 and DMEM media, respectively, both supplemented with 10% fatal bovine serum (FBS) and 100 U/mL of penicillin-streptomycin. The cells were incubated at 37 °C in a humidified environment with 5% $CO_2$. When the cells reached 80% confluence, they were detached using 0.25% trypsin-EDTA. For subsequent experiments, the cells were collected, centrifuged, and re-suspended in the growth medium.[19,30, 31]


© 2023 Wiley-VCH GmbH

23656549, 2023, 39, Downloaded from https://chemistry-europe.onlinelibrary.wiley.com/doi/10.1002/slct.202302448 by Bezm-I Alem Vakif University, Wiley Online Library on [01/11/2023]. See the Terms and Conditions (https://onlinelibrary.wiley.com/terms-and-conditions) on Wiley Online Library for rules of use; OA articles are governed by the applicable Creative Commons License

### MTT Assay to Determination of Cell Viability

To determine the cytotoxicity of the synthesized compounds (**4-21**), MTT (3-(4,5-dimethylthiazol-2-yl)-2,5-diphenyltetrazolium bromide) assays were performed on the HUVEC (human umbilical vein endothelial cell line) and HCT-116 (human colon cancer cell line) cell lines using nine different concentrations (250, 125, 64, 32, 16, 8, 4, 2, and 1 μM) of each compound. The stock solution of the reference drugs and target compounds were prepared as to be 10 mM concentration in DMSO and then they diluted desired concentration. The assay was performed by seeding $5x10^3$ cells into a flat-bottom 96-well plate with growth medium and incubating them for 24 hours. The cells were then treated with increasing doses of the compounds for an additional 24 hours, after which the assay was conducted. The absorbance values were measured at 540 nm using an Elisa microplate reader. The experiments were conducted in triplicate and the results were presented as the mean ± standard deviation. A concentration-dependent graph was generated by comparing the data for each compound, which was measured at least 3 times, and the relative % cell viability was calculated.[31,32] To determine the cytotoxic effect of compounds on cell viability, cells that were not treated with compounds were considered as 100% viable and cell viability was calculated according to the following formula; % Cell Viability = Sample/Control×100.[11,18,33]

### Molecular Docking Studies

*In silico* studies were performed using Maestro 13.5 program of Schrödinger Molecular Modelling Suite. Initially, the X-ray crystal structures of target proteins were obtained from RCSB Protein Data Bank: VEGFR2 (PDB ID: 4ASE), and TGF-β2 (PDB ID: 5QIN). Schrödinger's Protein Preparation Wizard was used to protein preparation studies. Maestro's Receptor Grid Generation was used to definite the binding site of each receptor. MM-GBSA module was used to calculate ligand-protein binding affinity. The compounds were drawn by using ChemDraw and were copied to Schrödinger. The optimization studies of the compounds were carried out by using Maestro's LigPrep software. Afterwards, all the compounds were docked utilizing Glide/XP interface.[9,10,34]

### Molecular Dynamics Simulations

Molecular dynamics simulations were carried out using Desmond (D. E. Shaw Research) According to the molecular docking results, the molecule with the highest binding score was selected and merged with the related enzyme. Protein ligand complex was prepared using the Desmond system builder module, and they were positioned at the center of an orthorhombic box with a 10 Å buffer zone between the protein and the box boundaries. To create a solvated and neutral system, water molecules (Tip3p) and counter ions (NaCl at 0.15 M) were added. The system was then optimized through energy minimization using the OPLS3 force field. The complex was loaded to the Desmond molecular dynamics module and the simulation of the system was performed for 50 ns under constant temperature (300 K) and pressure (1 bar) using with default parameters. The simulation was run, with a time step of 2.5 ps and using the RESPA integrator. The interactions between the ligand and protein during the binding were analyzed, as well as the RMSD, of the Cα atoms of the protein and the heavy atoms of the ligand, by utilizing Desmond.[35–38]

### In silico ADME Studies

The *in silico* ADME properties of the selected compounds were performed utilized the QikProp panel of Maestro 13.5. QikProp provides values that compare the properties of new molecules to 95% of known drugs.[9]

## Supporting Information Summary

NMR ($^1$H, $^{13}$C-APT, $^{19}$F, HSQC and HMBC), HRMS and FT-IR spectra of all the synthesized compounds (**2–21**) are available as supporting material. Furthermore, the cell viability graphics of biological activity studies were given in supporting material.

## Acknowledgements

This study was financially supported by Bezmialem Vakif University (Scientific Research Project Number: 20230212).

## Conflict of Interests

The authors declared no potential conflicts of interest with respect to the research, authorship, and publication of this article.

The authors declare that they have no known competing financial interests or personal relationships that could have appeared to influence the work reported in this paper.

## Data Availability Statement

The data that support the findings of this study are available in the supplementary material of this article.

**Keywords:** ADME · Anti-cancer · molecular docking · molecular dynamics · thiophene-2-carbohydrazide,

[1] D. M. Hausman, *Perspect. Biol. Med.* **2019**, *62*, 778–784.
[2] H. Sung, J. Ferlay, R. L. Siegel, M. Laversanne, I. Soerjomataram, A. Jemal, F. Bray, *Ca-Cancer J. Clin.* **2021**, *71*, 209–249.
[3] J. Massagué, *Cell* **2008**, *134*, 215–230.
[4] C. J. David, J. Massagué, *Nat. Rev. Mol. Cell Biol.* **2018**, *19*, 419–435.
[5] S. Saikia, M. Bordoloi, *Curr. Drug Targets* **2019**, *20*, 501–521.
[6] Archna, S. Pathania, P. A. Chawla, *Bioorg. Chem.* **2020**, *101*, 104026.
[7] R. M. da Cruz, F. J. Mendonça-Junior, N. B. de Mélo, L. Scotti, R. S. de Araújo, R. N. de Almeida, R. O. de Moura, *Pharmaceuticals* **2021**, *14*, 692.
[8] J. J. Court, C. Poisson, A. Ardzinski, D. Bilimoria, L. Chan, K. Chandupatla, N. Chauret, P. N. Collier, S. K. Dasi, F. Denis, W. Dorsch, G. Iyer, D. Lauffer, L. L'Heureux, P. Li, B. S. Luisi, N. Mani, S. Nanthakumar, O. Nicolas, B. G. Rao, S. Ronkin, S. Selliah, R. S. Shawgo, Q. Tang, N. D. Waal, C. G. Yannopoulos, J. Green, *J. Med. Chem.* **2016**, *59*, 6293–6302.
[9] H. Şenol, A. G. Ağgül, S. Atasoy, N. U. Güzeldemirci, *J. Mol. Struct.* **2023**, *1283*, 135247.
[10] F. S. Tokalı, H. Şenol, Ş. Bulut, E. Hacıosmanoğlu-Aldoğan, *J. Mol. Struct.* **2023**, *1282*, 135176.
[11] H. Şenol, R. B. Şahin, B. Mercümek, H. B. Kapucu, E. Hacıosmanoğlu, H. Dinç, P. Yüksel Mayda, *Nat. Prod. Res.* **2023**, *37*, 2500–2507.


© 2023 Wiley-VCH GmbH

23656549, 2023, 39, Downloaded from https://chemistry-europe.onlinelibrary.wiley.com/doi/10.1002/slct.202302448 by Bezm-I Alem Vakif University, Wiley Online Library on [01/11/2023]. See the Terms and Conditions (https://onlinelibrary.wiley.com/terms-and-conditions) on Wiley Online Library for rules of use; OA articles are governed by the applicable Creative Commons License

[12] A. R. Todeschini, A. L. P. De Miranda, K. C. M. da Silva, S. C. Parrini, E. J. Barreiro, *Eur. J. Med. Chem.* **1998**, *33*, 189–199.
[13] M. D. Altıntop, A. Özdemir, G. Turan-Zitouni, S. Ilgın, Ö. Atlı, G. İşcan, Z. A. Kaplancıklı, *Eur. J. Med. Chem.* **2012**, *58*, 299–307.
[14] M. Asif, A. Husain, *J. Appl. Chem.* **2013**, *2013*, 01–07.
[15] P. Melnyk, V. Leroux, C. Sergheraert, P. Grellier, *Bioorg. Med. Chem. Lett.* **2006**, *16*, 31–35.
[16] K.-K. Bedia, O. Elçin, U. Seda, K. Fatma, S. Nathaly, R. Sevim, A. Dimoglo, *Eur. J. Med. Chem.* **2006**, *41*, 1253–1261.
[17] F. S. Tokalı, P. Taslimi, I. H. Demircioglu, M. Karaman, M. S. Gultekin, I. Gulcin, K. Sendil, *Arch. Pharm.* **2021**, *354*, 2000455.
[18] F. S. Tokalı, H. Şenol, T. G. Katmerlikaya, A. Dağ, K. Şendil, *J. Heterocycl. Chem.* **2023**, *60*, 645–656.
[19] H. Şenol, B. Mercümek, R. B. Şahin, H. B. Kapucu, E. Hacıosmanoğlu, *Res. Chem.* **2022**, *4*, 100317.
[20] A. V. Afonin, I. A. Ushakov, D. V. Pavlov, O. V. Petrova, L. N. Sobenina, A. I. Mikhaleva, B. A. Trofimov, *J. Fluorine Chem.* **2013**, *145*, 51–57.
[21] Y. R. Consolacion, C. C. Esperanza, B. T. Oscar, B. Adiel Inah, L. E. Dinah, D. R. Dennis, S. Chien-Chang, *Pharmacognosy Res.* **2015**, *7*, 138–147.
[22] Y.-H. Feng, C.-J. Tsao, C.-L. Wu, J.-G. Chang, P.-J. Lu, K.-T. Yeh, G.-S. Shieh, A.-L. Shiau, J.-C. Lee, *Cancer Sci.* **2010**, *101*, 2033–2038.
[23] H. Nada, K. Lee, L. Gotina, A. N. Pae, A. Elkamhawy, *Comput. Biol. Med.* **2022**, *142*, 105217.
[24] N. Kılınç, M. Açar, S. Tuncay, F. Ö. Karasakal, *Lett. Drug Des. Discovery* **2022**, *19*, 996–1006.
[25] I. Shafique, A. Saeed, A. Ahmed, G. Shabir, A. Ul-Hamıd, A. Khan, B. Tüzün, M. Kirici, P. Taslimi, M. Latif, *Res. Chem.* **2022**, *4*, 100656.
[26] C. A. Lipinski, *Drug Discovery Today Technol.* **2004**, *1*, 337–341.
[27] W. L. Jorgensen, E. M. Duffy, *Adv. Drug Delivery Rev.* **2002**, *54*, 355–366.
[28] C. A. Lipinski, F. Lombardo, B. W. Dominy, P. J. Feeney, *Adv. Drug Delivery Rev.* **1997**, *23*, 3–25.
[29] A. G. Ağgül, N. Uzun, M. Kuzu, P. Taslimi, I. Gulcin, *Arch. Pharm.* **2022**, *355*, e2100476.
[30] H. Şenol, Ö. Özgun-Acar, A. Dağ, A. Eken, H. Güner, Z. G. Aykut, G. Topçu, A. Şen, *J. Nat. Prod.* **2023**, *86*, 103–118.
[31] H. Şenol, K. Çokuludağ, A. S. Aktaş, S. Atasoy, A. Dağ, G. Topçu, *Org. Commun.* **2020**, *13*, 114–126.
[32] S. Tuncay, H. Şenol, E. M. Güler, N. Öcal, H. Seçen, A. Koçyiğit, G. Topçu, *Med. Chem.* **2018**, *14*, 617–625.
[33] H. Şenol, A. G. Ağgül, S. Atasoy, *ChemistrySelect* **2023**, *8*, e202300481.
[34] H. Şenol, M. Ghaffari-Moghaddam, Ş. Bulut, F. Akbaş, A. Köse, G. Topçu, *Chem. Biodivers.* **2023**, *20*, e202301089.
[35] S. Carradori, A. Ammazzalorso, B. De Filippis, A. F. Şahin, A. Akdemir, A. Orekhova, G. Bonincontro, G. Simonetti, *Antibiotics* **2022**, *11*, 1375.
[36] N. Gariganti, S. K. Loke, E. Pagadala, P. Chinta, B. Poola, P. Chetti, A. Bansal, B. Ramachandran, V. Srinivasadesikan, R. K. Kottalanka, *J. Mol. Struct.* **2023**, *1273*, 134250.
[37] H. Şenol, Z. Çağman, T. G. Katmerlikaya, F. S. Tokalı, *Chem. Biodiversity* **2023**, *20*, e202300773.
[38] F. S. Tokalı, P. Taslimi, M. Sadeghi, H. Şenol, *ChemistrySelect* **2023**, *8*, e202301158.

Manuscript received: June 21, 2023


© 2023 Wiley-VCH GmbH

23656549, 2023, 39, Downloaded from https://chemistry-europe.onlinelibrary.wiley.com/doi/10.1002/slct.202302448 by Bezm-I Alem Vakif University, Wiley Online Library on [01/11/2023]. See the Terms and Conditions (https://onlinelibrary.wiley.com/terms-and-conditions) on Wiley Online Library for rules of use; OA articles are governed by the applicable Creative Commons License